^{1}H NMR spectral study of UV treated live *E. Coli* Bacteria

By

Michael Sorokopud

Thesis submitted in partial fulfillment of the requirements of the degree of Masters of Science in Physics

Department of Physics
Lakehead University
Thunder Bay, Ontario
May 7, 2010

Supervisor: Dr. Patrick Rapley, FCCPM
Co. Supervisors: Dr. Werder Keeler

Your file Votre référence
ISBN: 978-0-494-71756-1
Our file Notre référence
ISBN: 978-0-494-71756-1

Abstract

The lethal effects of ultraviolet radiation on microorganisms have been known and utilized for many years. In sufficiently high photon fluences, light and in particular, UV light, is an effective and subtle means of killing or at least immobilizing most, if not all cells and micro-organisms. Because of their small size, light can penetrate the enclosing protective walls and enter the inner volumes where it can break organic bonds in components that are vital to cell function. Despite the fact that a very low dose of UV light (1-9 mJ/cm^2) has been shown to inactivate many micro-organisms, there remains a dearth of biological information about light induced effects in molecules and their interactions within living microbial systems.

The use of ^1H NMR as a spectroscopic tool was chosen to undertake an examination of the possible effects resulting from exposing *E. coli* to lethal fluencies of UV radiation. Once sample preparation, treatment, and NMR mounting methods were optimized, the high sensitivity and high resolution capabilities of the method produced reproducible results for a series of experiments. These results reveal significant changes in the ratio of the ^1H NMR spectra of the treated to untreated *E.coli* samples when the treated sample was exposed to a lethal fluence of 275nm light. Photons at the 275nm wavelength, used in this study, have enough energy to break all of the principle bonds in an organic molecule. The difference spectrum between treated to untreated samples appears to be fitted well using specific component spectra from these groups of compounds. Increases in NMR peak amplitudes are observed and appear to be correlated with the spectral locations of several amino acids, membrane components and several sugars/saccharides. Increases in peak intensities of 4-8% were observed in the 0.8-1.1 ppm chemical shift region, characteristic of lipid and amino acid groups. A 3.5-4% increase was observed in the 2 ppm and 3.4-4 ppm region characteristic of various sugars and possibly amino acid components.

Acknowledgments

I would like to thank my supervisor and co-supervisor Dr. Patrick Rapley and Dr. Werden Keeler for all the help and guidance you both have provided me during this thesis. Dr. Rapley, thank you for providing me the opportunity to work on this project as well as the continual support throughout. Dr. Keeler, thank you for the use and access to the optics lab and all necessary equipment to perform this research. Your advice and guidance throughout this project have been invaluable. I am truly grateful for the many hours spent teaching me the intricacies of experimental research. Thank you to Dr. Leung for providing access to the microbiology laboratory, the supplies and for teaching me the necessary techniques to successfully work with microorganisms. As well, I would like to thank Keith Pringnitz and the Lakehead University Instrumentation Laboratory for providing me with the training and access to the NMR spectrometer. Your time was greatly appreciated. Finally, thank you to my wife Tiffany and family for all the support and patience you have shown me over the last two years, without you this would not have been possible.

Table of Contents

Table of Figures

List of Tables

Chapter 1: Introduction

1.1 Overview

In sufficiently high photon fluences, light and in particular, UV light, is an effective and subtle means of killing or at least immobilize all biological cell types, and most, if not all micro-organisms. Because of the small size of these organisms, light can penetrate the enclosing protective walls and enter the inner cell volumes where it can break organic bonds in molecular components that are vital to the maintenance of cell function. Once sufficiently damaged, even reproductive function can be curtailed. While the physics of this process seems straightforward enough, there has been surprisingly little research published studying this process. The use of UV light alone or in combination with other biologically destructive agents such as radiation, chemicals, antibiotics and other measures is a field that should be pursued as new techniques in the treatment of pathogens, cancers and other disorders may be developed. However, because of the dearth of biological information about light induced effects in molecules and their interactions within living microbial systems, the potential of the broader field remains largely untapped. An important approach in investigating changes in molecular systems is the use of spectroscopic methods. Because lethal UV photon fluxes to species such as bacteria are as low as a few tens of millijoules per centimeter squared of sample area, the spectroscopy chosen must be highly sensitive and capable of measuring changes in the environment of one or more of the 6 principle atoms in organic molecules.

The most widely used and locally available options are, Raman, FTIR and NMR. The sensitivity requirement rules out Raman and solvent constraints strongly favor the use of NMR over FT-IR. In an earlier study, attempts to quantify spectral changes induced by such fluences of light using FT-IR proved to be inconclusive due to desiccation problems (Vermeulen, 2006). Raman spectroscopy is even less practical as the optical measurement process is at least as damaging as any treatment used.

Of the six principle atoms in organic molecules, H, C, P, O, N & S, the first four of these are candidates for NMR spectroscopy using H^{1}, C^{13}(1.07% abundance), N^{15}(0.37% abundance) or P^{31}. Of these alternatives, hydrogen (^{1}H) is the most abundant atom in organic molecules

thus yields the strongest signal and may be able to determine the effects arising from changes in bonding between atoms and molecular groups resulting from treatment.

1.2 *Escherichia coli*

1.2.1 Introduction

A study of bacteria can be of interest in its own right. Bacteria serve as simple models for evaluating more complex cells and their function and thus, a study of *E. coli* may provide useful data for a future study of more complex cell types, including human cell lines or cancer cells. The biological properties of a few strains of *E. coli* have been studied for many years and are well documented. A large number of strains of *E. coli* exist, each having unique properties useful for studying biological function. For example, different strains of *E. coli* can differ in their deoxyribonucleic acid (DNA) makeup. Some strains share as little as 50% of their DNA in common with each other (Alberts et al. 2008), enabling comparisons to determine gene function.

E. coli are relatively easy to culture in simple nutrient broth and their short cycle period (approximately 30 minutes) permits a large number of bacteria to be grown in a relatively small time. This property also enables an *E. coli* sample to be re-cultured quickly to determine the number of viable cells after a specific treatment. By comparison, the cycle time of most eukaryote cells varies from approximately 30 hours (cancer cells) to many months (Alberts et al. 2008). Consequently, eukaryotic cell re-culturing is a much more difficult method for quantifying their response to external factors.

Although there are some *E. coli* strains that are pathogenic (strain 0157 is associated with food poisoning; (Betts, 2000)), most strains are non-pathogenic, making them relatively safe to work with. This thesis will focus on K12 *E. coli* bacteria strain in combination with ^{1}H NMR spectroscopy in an attempt to observe effects of the damage induced by exposure to known lethal doses of light at a given wavelength. Once lethal dose information is available for a cancer cell line, one could use a similar method to deduce the effects rendered there by UV or

short wavelength visible light. By extension the study of light in combination with other factors such as radiation therapy, chemotherapy or heat could also be undertaken.

1.2.2 Cell Structure and Composition

E. coli has a prokaryotic cell structure, meaning the cell consists of a multilayered cell membrane and a nuclear body lacking internal membrane structures. This simplified cell structure is one reason prokaryotic organisms have the ability to grow rapidly, with a doubling time of as little as 20 to 30 minutes.

Approximately 70% of the *E. coli* cell mass is water. The remaining macromolecules and their dry percentage weights (Ingraham, Maaloe, & Neidhardt, 1983) are listed in Table 1.

Macromolecule	Percentage of total dry weight
Protein (Amino Acids)	55
RNA	20.5
DNA	3.1
Lipids	9.1
Lipopolysacchrides	3.4
Peptidoglycan	2.5
Glycogen	2.5

Table 1 Macromolecular composition of an average *E. coli* cell

Along with these macromolecules, there are also trace amounts of vitamins, metabolite building blocks and inorganic ions.

1.2.3 Lipid Component of the Bacterium

The complex cell wall of Gram negative prokaryotic organisms (vs. the simpler cell walls of Gram positive bacteria) is composed of two phospholipid bilayers and a peptidoglycan layer. A cross section showing the outer membrane, the periplasmic space and the inner membrane is illustrated in Figure 1.

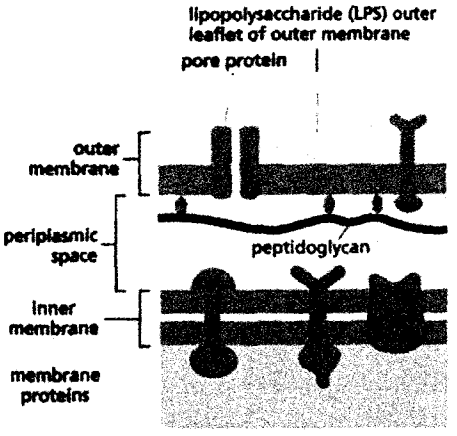

Figure 1 Gram negative bacteria cell membrane structure (Alberts, Johnson, Lewis, Raff, Roberts, & Walter, 2008)

The inner and outer membranes are composed of three major phospholipids; phosphatidylethanolamine, phosphatidylglycerol and cardiolipin (Ames, 1968) in order of decreasing concentration. Trace amounts of phosphatidylserine are also present (Ingraham, Maaloe, & Neidhardt, 1983). The molecular structure of these phospholipids is illustrated in Figure 2.

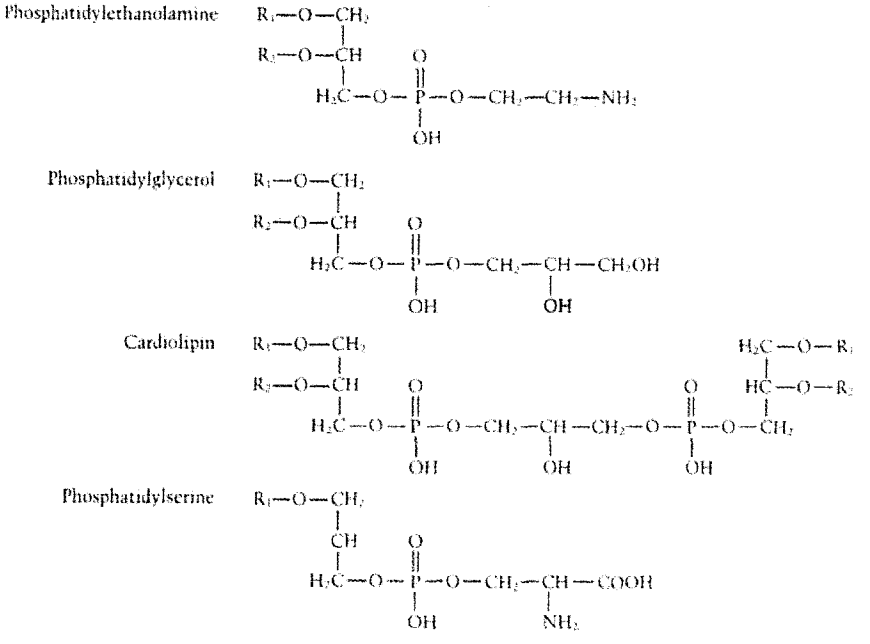

Figure 2 Phospholipid structure, R1 and R2 = fatty acid residues (Ingraham, Maaloe, & Neidhardt, 1983)

Phospholipids in the *E. coli* membrane will primarily bind to four fatty acids: palmic, palmitolic, Methylenehexadecanoic and cis-vaccenic acid. The fatty acids bind to the phospholipids at the R1 and R2 locations. The molecular structure of these common fatty acids is illustrated in Figure 3.

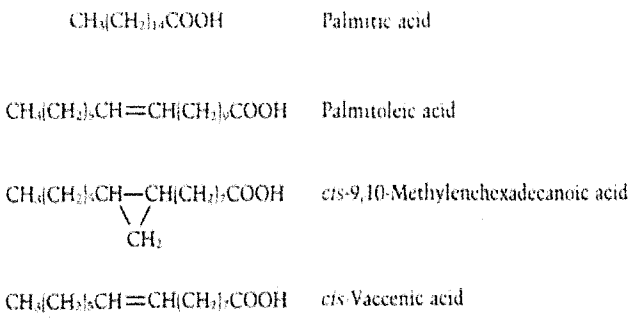

Figure 3 Structure of common fatty acids (Ingraham, Maaloe, & Neidhardt, 1983)

The surface layer of the outer membrane contains lipopolysacchrides, which are long macromolecules projected outward from the cell. A variety of proteins are also present in the structure of the inner and outer membrane. The outer membrane has 20 – 30 proteins which are thought to alter the permeability of the membrane. The cell membrane, which can amount to 70% of the overall membrane mass, is the final enclosing structure and is made up of a phospholipid bilayer, and proteins, many of which regulate the molecules entering and leaving the cell. Apart from this transport function, little is known about how the cell membrane is involved in the metabolic processes within the cell.

1.2.4 The DNA/RNA Components of the Bacterium

The central region of prokaryote cells, termed the nuclear body, contains a variety of biological structures including deoxyribonucleic acid (DNA), ribonucleic acid (RNA), ribosomes, proteins, and cytoplasm. As with many bacteria, the DNA in *E. coli* is present as a single circular chromosome containing approximately 4.6 million nucleotide pairs. Each nucleotide consists of a five carbon sugar backbone bound to a ring structure referred to as the base. Thymine (T) and cytosine (C) are pyrimidines, which consist of a six-member carbon ring structure with a nitrogen atom at position 1 and 3. Guanine (G) and adenine (A) are purines, which are composed of a pyrimidine ring fused to a five- member carbon ring structure with nitrogen

atoms located at locations 7 and 9 (Alberts et al. 2008). The four bases are illustrated in Figure 4.

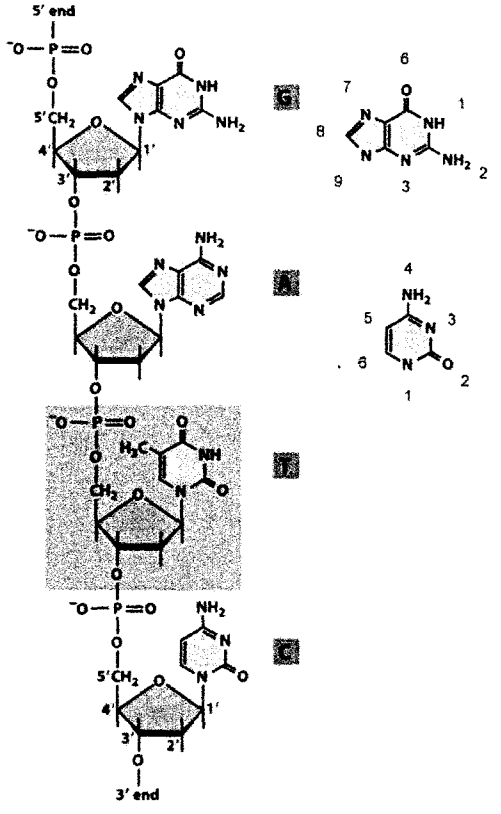

Figure 4 (left) Atomic composition of the four DNA Base molecules, (right) Numbering scheme of the purine and pyrimidine rings(Alberts et al. 2008)

Each base will bind to a complimentary base forming a double stranded molecule which forms a double helix structure. In *E. coli* long DNA molecules form loop domains which radiate from a central point, allowing the DNA molecule to exist as a highly condensed structure that frequently occupies a distinct region of the cell (Thanbichler, Wang, & Shapiro, 2005).

1.2.5 The Protein Components in the Bacterium

The largest fraction of bacterial mass (excluding water) is composed of protein material. The two primary functions proteins serve are catalysts (in the form of enzymes) to increase the rate of chemical reactions within the cell, and structural proteins. Proteins are composed of many amino acids covalently linked together via peptide bonds. This chain of amino acids will fold into a variety of complex structures held together by hydrogen bonds between nearby

amino acids (Madigan, Martinko, & Parker, 2003). Since proteins are assembled from amino acids, one expects the protein ^{1}H NMR signal to be dominated by the most common H bonded assemblies in the acids. From an inspection of the Figure 5, it appears that CH_2 bonds might dominate the H bond groups with significant contributions from NH, NH_2, OH, and carbon ring structures.

Figure 5 shows the 21 amino acids for reference purposes. The *E. coli* bacterium can synthesize most of the amino acids required for cell growth and function from the presence of glutamine (Ingraham, Maaloe, & Neidhardt, 1983).

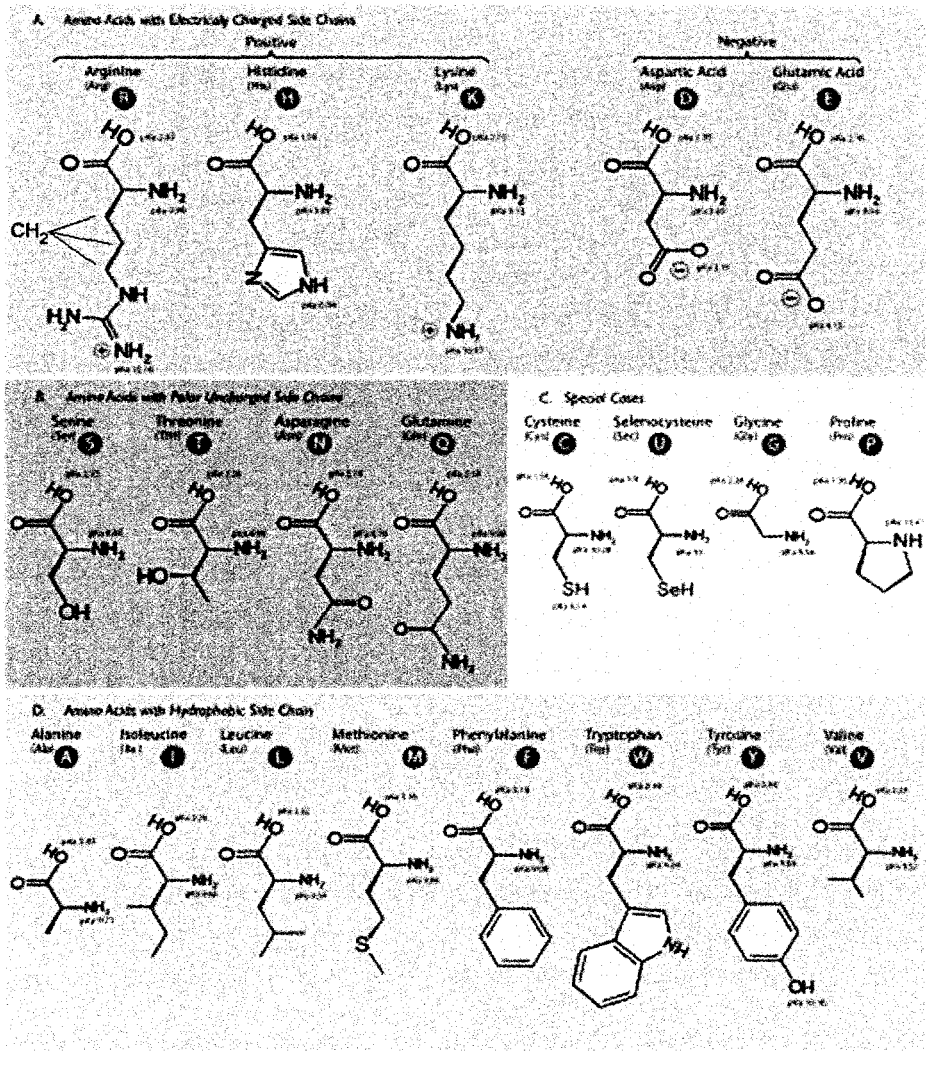

Figure 5 Table of amino acid structures with CH_2 bonds labeled (CRC handbook of chemistry, 2010)

1.3 Bactericidal Effect of Ultraviolet Radiation on *E. Coli*

1.3.1 Introduction

The lethal effects of UV radiation on microorganisms have been known and utilized for many years. Today, UV light is being used for sterilization in a variety of areas. Drinking water sterilization by UV radiation is becoming a common step at water treatment facilities and in well water filtration systems. On a smaller scale, there are now a variety of consumer products available where UV lamps are used to sterilize air, surfaces and small quantities of drinking water. A relatively low dose of UV (1-9 mJ/cm^2) has been shown to inactivate 99-99.9% of *cryptosporidium parvum* oocysts and *giardia lamblic* cysts (Betancourt & Rose, 2004), both of which can be found in contaminated drinking water and are resistant to chemical disinfection processes. Data is also available showing that a relatively low dose is required to kill a wide variety of bacteria, viruses and protozoan in water (Hijnen, Beerendonk, & Medema, 2006). Another advantage of using UV radiation to inactivate a variety of microorganisms is that unlike chemical sterilization processes, it is impossible to over treat when using UV light, and UV treatment occurs without leaving undesirable by-products or chemical residues (Chang, et al., 1985).

Although UV sterilization products are becoming more popular, there are still many questions regarding the interaction of UV radiation with biological systems. To further complicate the subject, many studies use broad spectrum lamps. Exposing samples to such a broad spectrum of light makes it difficult to determine the damage done by a particular wavelength, and the exact mechanism that causes the observed lethal effect.

1.3.2 Potential Lethal Mechanism Involving UV radiation

The energies required to break specific bonds involving the six main elements in an organic system are listed in Table 2 (Vermeulen, Keeler, Nandakumar, & Leung, 2007). Included is the equivalent photon wavelength for each. Lethal dose data as a function of wavelength has been determined for *E. coli* and the wavelength dependence was observed to be a strong exponential (Vermeulen, Keeler, Nandakumar, & Leung, 2007).

Bond	Energy (eV/bond)	Equivalent Photon Wavelength(nm)
O-H	4.772	259.80
P-O	4.338	285.78
C-H	4.252	291.58
N-H	4.035	307.39
C-O	3.644	340.22
C-C	3.601	344.32
S-H	3.514	352.82
C-N	3.037	408.26
C-S	2.690	460.94
N-O	2.299	539.21
S-S	2.213	560.36

Table 2 Organic bond breaking energies and equivalent wavelength

From published bactericidal data in the literature, it is suggested that UV effects on the cells can occur in many ways including DNA and RNA damage, membrane perforation and damage to or disruption of enzyme and protein function including membrane transport proteins (Jagger, 1981).

Research into the mechanism responsible for the bactericidal effects of UV radiation have centered on the mutations and damage to the organism's DNA. Being essential to the functioning and reproduction of the cell, damage or modification to this molecule will result in loss of functionality, or cell death if the damage or mutations cannot be repaired. Due to the heterocyclic aromatic structure of nucleotides, it was shown early on that they are an effective absorber of UV radiation (Jagger, 1967). They postulate the primary effect of the absorbed photons is the production of DNA lesions which commonly form between two adjacent pyrimidine bases (cytosine and thymine). These pyrimidine dimers, can occur in two forms: cyclobutane pyrimidine dimer (CPD) and 6,4 pyrimidine pyrimidone (6-4PP).

CPD's are the most abundant DNA lesion present after UV irradiation and thought to be the most cytotoxic (Sinha & Hader, 2002). The lesions form after the absorption of a UV photon which causes the carbon atoms at locations 4 and 5 to bond with the carbon atoms at the same locations of an adjacent pyrimidine. These new bonds form a 4 atom carbon ring between adjacent pyrimidines. 6-4PP are formed by the bonding of carbon atoms located at position 4

on the 5' pyrimidine and location 6 on the 3' pyrimidine (Matsumura & Ananthaswamy, 2002). Both types of DNA lesions form a kink on one side of the DNA double helix. CPD account for approximately 75% of the lesions produced while 6-4PP lesions account for 25% (Sinha & Hader, 2002). Both lesions inhibit DNA transcription replication within a cell which can lead to the loss of protein and enzyme function and cell death if sufficient lesions are able to accumulate.

Another possible mechanism responsible for inducing damage to biological molecules is a group of small molecules called reactive oxygen species (ROS). Although naturally occurring as a result of metabolic activity, exposure of bacteria to UV radiation has been observed to increase the concentration of reactive oxygen species within a cell. These small molecules can include superoxide anion(O_2^-), hydroxyl radicals(HO), hydrogen peroxide(H_2O_2) and singlet oxygen (Zhang, Rosenstein, Wang, Lebwohl, & Wei, 1997). Examples of the potential damage caused by the over generation of ROS includes; single strand breaks in the DNA molecule, liberation of the DNA bases from the sugar backbone caused by hydrogen peroxide ROS (Ananthaswamy & Eisenstark, 1977), as well as lipid, protein, and DNA damage from reactions with singlet oxygen. When interacting with the DNA molecule, singlet oxygen can produce mutations which lead to the miss pairing of base pairs (Cavalcante, Martinez, Mascio, Menck, & Agnez-Lima, 2002). ROS have also been implicated in double strand DNA breaks and the disruption of membrane transport function.

Bacteria are regularly exposed to low doses of UV radiation and appear to have developed a variety of mechanisms to repair damage induced by the radiation. The photolyase enzyme specifically binds to either CPDs or 6-4PP lesions, and can reverse the damage under exposure to visible light. In the absence of light, a combination of proteins can recognize a lesion in the DNA strand, excise the dimer, and fill the gap (Sinha & Hader, 2002). Repair mechanisms also exist for single and double strand DNA breaks. As seen earlier, UV radiation (depending on the wavelength) has the ability to break many, or all of the bonds present in a biological system. This implies that under a larger dose of the UV radiation, the enzymes

responsible for the repair of DNA and other macromolecules are themselves susceptible to damage, rendering them ineffective in that case.

At present, there is no definitive proof to favor one or more of the suggested mechanisms in the bactericidal effects of UV. It is hoped that a ^{1}H NMR spectroscopic comparison of UV treated vs. untreated samples might help in determining major causes for the bactericidal action of the UV. Because of the possibility of photon bond breaking or disruptive interactions with most molecules inside the cell, additional mechanisms are possible such as perforated of membrane walls, deterioration of protein mass, or the general cross-linking of bonds within the overall cell structure. These could all be contributing factors in the overall bactericidal effect.

1.4 ^{1}H NMR Spectroscopy

1.4.1 Introduction

The live bacteria in this study were exposed to a lethal fluence of UV radiation. It is hoped that this fluence might induce spectroscopically detectible changes within the cells. However, the lethal fluence of photons at 275nm, is quite small, being equivalent to exposing sample cells to the photon flux of a 3 mW laser pointer for only 1 to 2 seconds! Hence, the spectroscopic method chosen must be able to detect changes produced by this exposure. The choice of spectroscopic method must have:

- Non deleterious effects to live samples
- Very high sensitivity
- Relative insensitivity to sample environment (solvent)
- Rapid acquisition time (preferably a fraction of the 30 minute cell cycle time)

As was previously mentioned, IR spectroscopy and Raman spectroscopy were rejected because the former is too sensitive to the presence of water, and the latter is a much less sensitive method in general and damaging to the sample. While NMR was the best choice, proton NMR was chosen over carbon or phosphorus NMR because of the significantly higher signal strength associated with the higher proportion of NMR sensitive ^{1}H atoms in the small

sample mass. Replacement of H_2O with D_2O prior to measurement, helped to reduce the free solvent proton signal.

NMR spectroscopy is a non-destructive, non-invasive method to investigate the chemical composition of a sample. The method utilizes radio frequency (R.F.) radiation to probe the magnetic environment of nuclei with a non-zero nuclear spin. The nuclear energy levels of a ^1H (spin ½) nucleus, when placed in a strong magnetic field, will split into two states with energy

$$E = \mp\frac{1}{2}\gamma B_0 \text{ (Energy levels for spin 1/2 nucleus)} \qquad 1\text{-}1$$

where B_0 is the main magnetic field of the instrument and γ is the gyromagnetic ratio, an intrinsic property of the nucleus under investigation. The low energy state is populated with nuclear spins aligned parallel to the main magnetic field, and the high energy state is populated with spins aligned anti-parallel. The NMR signal is generated by the excess nuclear spins in the low energy state. The ratio of nuclei in the low to high state is governed by the Boltzmann equation

$$\frac{n}{n_h} = e^{\frac{\Delta E}{kT}} \text{ (Boltzmann equations)} \qquad 1\text{-}2$$

The value of $\frac{\Delta E}{kT}$ at a 11.7 T field strength at room temperature for the ^1H nucleus yields a ratio of approximately 8×10^{-5} (Chary & Govil, 2008). This means that for every 1,000,000 ^1H nuclei in the high energy state there are 1,000,080 nuclei available in the low energy state to generate a signal. At equilibrium, excess of spins aligned parallel to the field add vectorially to produce a magnetization vector, M_0, along the main field axis.

Another property observed when nuclei are placed into a magnetic field is the precession of the individual nuclear magnetic moments around the axis of the field. The angular frequency of precession or Larmor frequency, is given by

$$\omega_0 = \gamma B_0 \text{ (Larmor frequency)} \qquad 1\text{-}3$$

To obtain a NMR spectrum, a pulse of radio frequency (R.F.) radiation is applied to the sample to tip the magnetization vector into the plane, perpendicular to the magnetic field. After the application of the pulse, the nuclear magnetic moments are free to precess back to their equilibrium alignment. As this process occurs, the radiated electromagnetic field induces a current in the receiver coils which are recorded by the computer. The frequency with which the individual nuclei precess is altered by small changes in the local magnetic environment, known as the chemical shift. The detected signal is the sum of all ^{1}H precession frequencies present in the sample and is known as the free induction decay (FID) signal. ^{1}H NMR spectroscopy is particularly sensitive to changes in the local proton environment and can respond to changes induced by subtle treatment effects such as those associated with a small flux of photons.

The Larmor frequency of the nuclear magnetic moments is dependent on the main magnetic field of the instrument, and consequently different instruments will measure a different chemical shift making spectra from different instruments difficult to compare. To resolve this, all spectra are referenced to a chemical standard, the most common being tetramethylsilane according to the equation (Balci, 2005)

$$\delta(ppm) = \frac{\nu_{sample} - \nu_{standard}}{\nu_{spectrometer}} \times 10^6 \quad \text{(Chemical Shift)} \qquad 1\text{-}4$$

where δ is the chemical shift, $\nu_{sample}, \nu_{standard}(TSP), \nu_{spectrometer}(500MHz)$ are precession frequencies in Hertz. Chemical shifts are expressed in units of parts per million (ppm) frequency shifts relative to the reference. These are now magnetic field independent. When D_2O is used as a solvent, 3-(Trimethylsilyl) propanesulfonic acid (TSP) is typically used as the 0 ppm reference as TMS is insoluble in D_2O.

1.4.2 Pulse Sequencing

To probe the sample and determine its response spectrum, a square wave pulse is applied to the sample with the fundamental R.F. Fourier component near the resonance frequency of the desired nuclear type. Nuclei of that type absorb the energy and align the magnetization vector in the plane of the R.F. pulse. This pulse tips the nuclear magnet moments ≈90 degrees from the axis of the main instrumental magnetic field. After the pulse is absorbed,

the nuclei precess with their characteristic frequencies, back to the initial equilibrium orientation over a period of hundreds of milliseconds. The precession frequency of a given ^1H nucleus is determined by the externally applied magnetic field plus that due to the local, atomically generated magnetic environment. The intensity at a particular frequency of the precession induced NMR signal in a pickup coil, is directly proportional to the population of that particular nuclear type in that magnetic field environment. The characteristic of the applied pulse and their sequence delivery to the sample is determined by settings in the computer control software.

In this study, the bacterial samples are grown in a water based medium. While the non water ^1H signals occur at broadly different frequencies, the overwhelming intensity of the water signal must be significantly reduced if the other molecular species are to be observed. The very large H_2O peak at 4.65 ppm can be reduced by washing and suspending the cells within a NMR insensitive solution, such as D_2O and by using a pre-saturation pulse sequence technique. The pre-saturation pulse is a narrow band pulse located at 4.65 ppm. This pulse saturates possible absorption by the remaining free H_2O, selectively removing nuclei at that frequency from contributing to the magnetization vector so that the subsequent broadband pulse can interrogate the remaining species.

1.4.3 Signal Improvement

After washing and re-suspending the bacteria in high purity D_2O, the H_2O signal was reduced by orders of magnitude. The remaining water peak was further suppressed by applying a narrow-band pre-saturation pulse centered at the H_2O absorption frequency. When optimized in intensity and band width, this pulse pre-flips the still sizable remaining water signal so that there is less absorption in the subsequent wider-band spectrum pulse. The delay between the pre-saturation pulse and the acquisition pulse was also adjusted for optimal water signal reduction. The combination of D_2O wash and re-suspension, and a pre-saturation pulse is utilized in many biological NMR studies (King & Kuchel, 1994).

Finally, the signal to noise ratio was improved by co-adding the spectral scans in a given run. Noise signals from the spectrometer are random while signals from the sample are

repeatable. If the scans are repeated and the spectra summed, the sample signal will add while the noise adds randomly. By utilizing this technique the signal to noise ratio is approximately proportional to the square root of the number of scans summed (Levitt, 2006). When working with living, whole cells, there is a practical limit to the number of scans that can be acquired as cells can settle below the active sampling volume, centered about 1-3 cm from the bottom of the sample tube. The bacteria cells may be unable to survive extended periods suspended in D_2O.

1.4.4 Biological NMR

There have been very few ^1H NMR studies of intact biological specimens, and even fewer studies of living biological species under environmental stress. The primary focus of many biological NMR studies was on the investigation of biological building blocks such as amino acids, nucleic acids, proteins, lipids and other macromolecules. Most studies were carried out on purified cellular extracts in order to produce a more homogeneous sample and narrow the line widths of the resulting spectra. Furthermore, no NMR studies could be found in which the principle investigative parameter was exposure to light. This is somewhat surprising when one considers that it is well know that UV light is an excellent sterilizing agent for bacteria, viruses and protozoa and that commercial light based sterilizing products are widely available. It is generally assumed that the UV light damages the DNA in reproductive species, but as previously outlined, other mechanisms such as membrane perforation or protein and macromolecular damage, may be just as important.

Many biological NMR investigations to date have centered on protein studies enhanced by the addition of NMR sensitive tagged molecules. Other examples include the study of protein interaction, protein structure, lipid interactions and cellular metabolism. Cooper et al. (2001) utilized ^1H NMR spectroscopy to monitor visible lipids in eukaryotic cells before and after external chemical agents were added (Cooper et al. 2001). NMR spectroscopy is also being looked at as a method of detecting and monitoring apoptosis in eukaryote cells. Much of this research is focused on the increased ratio of the methylene (CH_2) peak (1.3 ppm) to methyl (CH_3) peak (0.9 ppm) detected in the lipid components of cells undergoing apoptosis (Brauer,

2003). This ratio has been observed to change depending on the cell line and the type of chemotherapeutic drug used to induce apoptosis in the cells (Mikhailenko, Philchenkov, & P, 2005). Studies strictly using UV radiation to induce apoptosis could not be found.

1.4.5 Advantages in Studying Living Cells Using ^{1}H NMR Spectroscopy

NMR spectroscopy is well suited for studying living cells. The data acquisition process is non-destructive to biological systems, enabling the study of intact cells and tissue over an extended period of time. Starting in the 'live' state, there is little concern about signal change due to sample decomposition with time. The RF radiation used in the pre-saturation and acquisition pulse is non-invasive and does not place stress on cells. ^{1}H NMR spectroscopy has further benefits in that it is the most sensitive nuclear choice for several reasons;

- 99.96 % of naturally occurring hydrogen is NMR sensitive ^{1}H (the remainder being deuterium), whereas for carbon, only 1.11% is ^{13}C
- The sensitivity of a nucleus is proportional to $\gamma^3(I+1)$ (King & Kuchel, 1994), with a gyromagnetic ratio of 2.674 (10^8 rad s^{-1} T^{-1}) (Balci, 2005), ^{1}H has a higher sensitivity that most other NMR sensitive nuclei.

Although ^{31}P has a 100 % natural abundance, the low concentration of ^{31}P (present mainly in cell metabolites) in biological systems makes phosphorus NMR difficult and limited to metabolic studies, while ^{1}H nuclei is present in all biological molecules in high concentrations.

1.4.6 Difficulties

NMR spectroscopy will yield the highest resolution for identical homogeneous samples of small molecules. To achieve this high resolution, most studies of cell components (proteins, lipids etc.) involve lysing (rupturing) and removing the cell wall. In whole live cell samples, the increased complexity of the full cellular structure and the mobility of molecular species due to metabolic activity, produce broad, overlapping peaks in the NMR spectra making interpretation difficult.

Cells grown in a water based broth and concentrated by centrifuging as the first step in the sample preparation, still present difficulties for ^{1}H NMR spectroscopy. If cells are kept

suspended in H_2O, the signal from the water molecules is many orders of magnitude higher than signals from organic molecules. Even with D_2O wash and re-suspension of cells and a pre-saturation pulse sequence, live bacterial samples still contain significant amounts of inter-cellular water which results in a large and broad peak in the resulting spectra.

E. coli cells have an inherently low concentration of dry organic mass when compared to the total sample volume. Each cell is composed of ~ 70% water, making a high cell concentration important for acquiring reasonable spectra. Because of the relatively short cell division time, *E. coli* suspension in high concentrations can be grown in a period of days or less. If the concentrations are made too high using centrifuge techniques, the bacterial cell will clump and then precipitate during the study period. Even with the highest usable concentration of suspended cells, co-adding of several hundred scans must be taken to produce spectra with a reasonable signal to noise ratio. Because of the high number of transients needed, samples become susceptible to contamination from a variety of source. Lower purity grades of D_2O (99%, 99.9%) (product number 435767-100G, 151882-125G) used early in this study contained unacceptably large and batch dependent amounts of impurities. The signal peaks from these impurities varied in spectral location, and were usually many times larger than the later discovered intrinsic signal due to the bacteria. The 99.96% D_2O (product number 151890-125G) proved to be virtually impurity free, except for a small H_2O peak. Since D_2O is hydroscopic, atmospheric absorption during UV treatment can introduce unequal amounts of H_2O into the sample along with contaminations when handling times are not identical. To obviate the atmospheric absorption problem during UV treatment, a high purity (99.996%) nitrogen purge gas flowed through the sample cell holder for the duration of the treatment. In order to ensure that the reference (non-UV exposed) sample was handled in an identical fashion, it too was placed in the purged same holder for an identical period of time

1.5 Research Objectives

This thesis will focus on the K12 *E. coli* strain in combination with 1H NMR spectroscopy in an attempt to quantify the damage induced by exposure to known lethal doses of light at a given wavelength. Specific research objectives undertaken to fulfill this goal are listed below;

i. Learn how to culture, wash and re-suspend bacterial cells

ii. Learn and use the drop plating method to evaluate the viability of cultured cells suspended in D_20 and exposed to various fluences of UV light

iii. To assemble a pseudo-monochromatic light system for treating the cells and to develop a method for mounting unexposed and UV exposed samples in NMR tubes for spectroscopic analysis, and

iv. To determine the quantitative changes in the NMR spectral peak groups and attempt to associate these changes with possible biological building blocks or molecular groups.

Once lethal dose information is available for a cancer cell line, one could use a similar method to deduce the effects rendered there by UV light. By extension, UV light in combination with other lethal factors such as radiation, chemotherapy, heat shock, or combinations thereof could be considered.

Chapter 2: Experimental

2.1 Introduction

To detect the expected small changes caused by UV radiation, the experimental procedure was revised many times in order to reduce contamination from various sources. Once contamination was minimized, a strict procedure was followed to guarantee reproducible sample to sample preparation, treatment and analysis. A chronological review of the significant changes to the experimental method is outlined in section 3.1. The following section outlines the experimental procedure used to acquire the spectra discussed in section 3.3.

2.2 Experimental Procedure

2.2.1 *E. Coli* Culturing

The *E. Coli* strain ATCC 25922, was obtained from the American Type Culture Collection (ATCC), and re-grown on a Trypticase soy agar (TSA) plate. A colony from the TSA plate is then cultured in a beaker containing Trypticase soy broth for 24 hours, in a 37^{O} C shaking incubator at 100 rpm. After incubation, 1.5ml of broth is washed twice in 0.5ml of 99.96% deuterium oxide (D_2O), then re-suspended in 1.0ml of 99.96% D_2O. Deuterium oxide has been shown to be only slightly toxic to live bacterial cells, and over the time period of our experiment, there were no observable effects based on the drop plate data obtained.

2.2.2 UV Source

UV light at 275nm was produced by focusing light from a 100W Hg lamp located at one foci of a Photonic Technology Inc.(PTI) on axis ellipsoidal mirror into the entrance port of a ¼ m Jarrell-Ash monochromator. Both the reflector mirror and spectrometer are F/4 for optimal solid angle coupling to the 250nm blazed grating inside the monochromator. Both entrance and exit slits of the monochromator were removed, leaving effective slit widths of approximately 8mm. While this provided maximum intensity at the output, the configuration resulted in an output dispersed bandwidth of approximately 10nm about the selected wavelength.

2.2.3 Optical Setup

Light emerging from the exit port of the monochromator was collected and collimated by a F/4 off-axis parabolic mirror. The collimated beam was then focused with a second, identical off-axis parabolic mirror where it could either be directed to the location of the sample treatment container, or to a chopped beam pyroelectric power meter for intensity determination. The optical setup with major components in treatment configuration is illustrated in Figure 6 and Figure 7

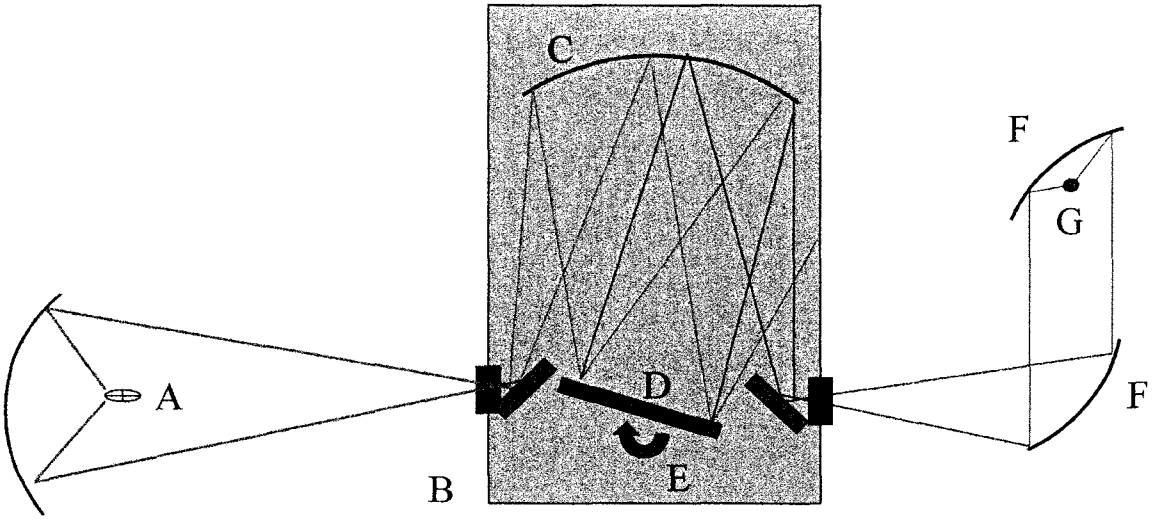

Figure 6 Optical path illustrating: (A)Arc lamp,(B)Ebert monochromator, (C)Spherical mirror, (D)250nm blazed grating, (E)Wavelength control gear,(F)Off axis parabolic mirrors,(G)Sample chamber

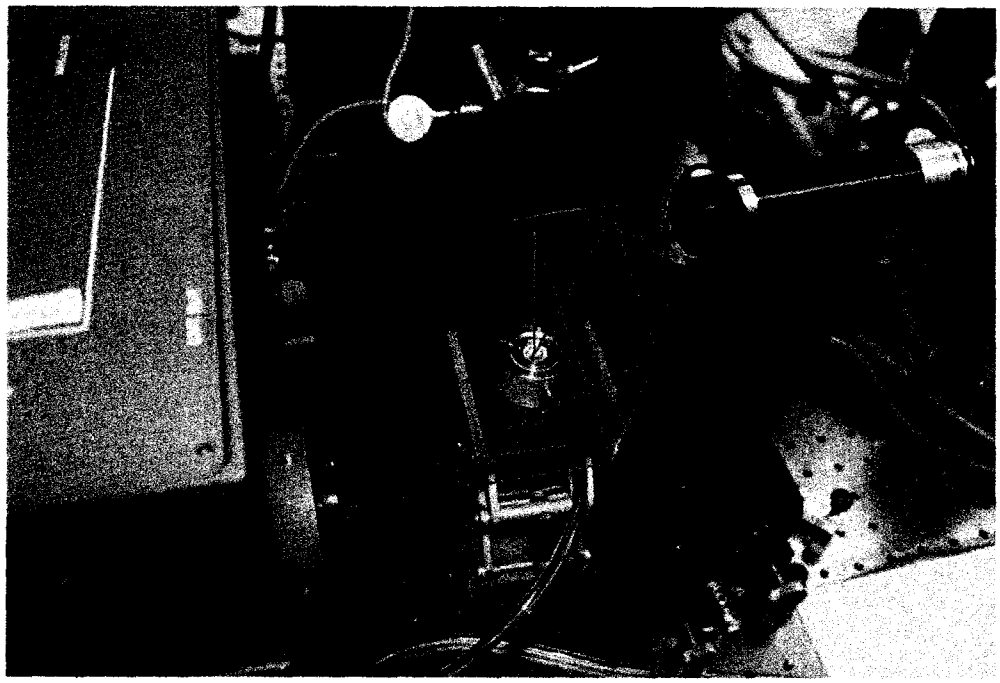

Figure 7 Optical setup, monochromator, off-axis parabolic mirrors, power mirror and sample chamber visible. Mirrors are configured for sample treatment with a simulated beam visible

The focused spot was approximately 0.8 cm wide 1.3 cm in length and closely overlapped the area of the sample treatment container. Because of the exit slit width, the dispersed output beam wavelength varies linearly across the sample by approximately 10 nm. The samples were rotated by 180 degrees, after 50% dose delivery, to improve homogeneity of energy distribution over the sample.

2.2.4 Treatment Sample Holder

The sample holder was the lower 4 mm of a 1 mL beaker and has an internal diameter of 7 mm. During treatment, the holder is mounted inside a machined aluminum block, which is sealed at the top with a sapphire window (Crystal Systems Inc.) whose transmisivity for 275nm light is 0.86. The entire sample chamber is illustrated below (Figure 8). Channels are cut into the lower sidewall of the block to permit the entire holder to be purged with high purity N_2 gas. This purging prevents adsorption of water vapor from the atmosphere as well as preventing air-born particles from contaminating the sample.

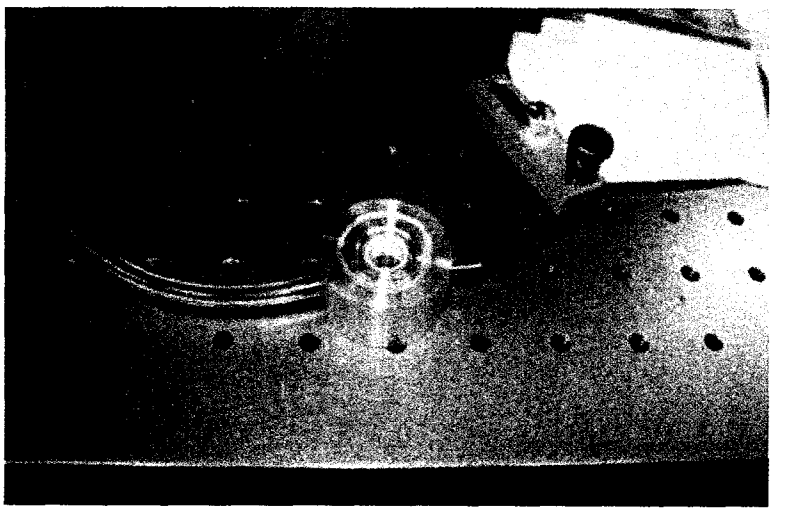

Figure 8 Sample Holder for UV Treatment

2.2.5 UV Treatment of *E. Coli*

Prior to treatment, the nominally 100W Hg lamp is powered up and given 20 minutes to stabilize. The power supply is then set to the normal operating current of 6A, and output voltage, which is set automatically by the controller, settles near 15V. The power at the sample was always determined using a model RKP-360 Laser Precision Inc. pyroelectric detector with its accompanying RL-3610 power meter. To avoid high 1/f noise present in a dc readout, the beam is chopped at the lock-in operating frequency of 30Hz. The power meter system is accurate to the microwatt level. Due to bulb aging over the course of this study, the Hg bulb output decreased slightly necessitating slightly longer treatment times. Thus final fluence at the sample is determined by the product of power density and exposure time.

White light reflected/scattered from the grating in the zeroth order is present in the output beam and comparable in power to that at 275nm. To determine the fraction of the output beam due to this white light, a thin glass cover slip or microscope slide placed in front of the detector, was used to absorb the UV component. Subtracting the white light reading, from the total provided a measure of the UV power present in the output beam. Since the white light wavelengths have extremely low killing power by factors of 10^{-3} to 10^{-8} (Vermeulen, Keeler, Nandakumar, & Leung, 2007) its presence during treatment can be ignored.

UV treatment of the sample occurred within one hour of washing and cell re-suspension in high purity D_2O. Except for brief pipetting periods, the samples were contained in sealed 1.5ml centrifuge tubes. The bacteria suspension was pipetted in single 100 µL volumes into the sample holder and placed into the beam for 5 minutes (bulb age corrected). This was repeated until 1mL of cell suspension was treated. An identical process was followed for a reference (unexposed) sample, so that the only difference between the sample and reference was the exposure to optical flux while in the purged chamber. 0.5 mL of each sample was pipette transferred to sealable 5mm NMR sample tubes, which had been previously cleaned and dried. The remaining 0.5 mL of sample was used for drop plate assay measurement.

2.2.6 Drop Plate Measurements

The mortality of the bacteria is verified in both the treated and reference (untreated) samples by drop plating the remaining 0.5 mL of bacteria suspensions. The drop plating procedure requires a serial dilution of the original sample material by up to eight factors of 10. The lowest concentration of cells is therefore a factor of 10^8 times more dilute than the original suspension. Five, 5 µL droplets from each dilution stage are placed onto TSA plates and then incubated. After incubation the number of colony forming units (CFU) is counted and the initial concentration of viable bacteria is calculated (Ingraham, Maaloe, & Neidhardt, 1983).

2.2.7 NMR Analysis

Proton ^1H NMR spectroscopy was performed using a Varian UNIY Inova 500 spectrometer system and Varian VNMRj acquisition software. Proton resonance was measured using a 5mm probe at an operating frequency of 499.72 MHz. In order to avoid settling of the bacteria cells within the sample tube, total scan time was limited to less than two hours. A presaturation pulse sequence with parameters listed in Table 3, was used to acquire the spectra with a minimized residual H_2O signal.

Pulse	Acquisition Time (s)	Recycle Delay (s)	Data Points/FID	Sweep Width (Hz)	Number of Transients
9.2 µsec 90° spin-angle flip	3.34	1.0	1000	3000	1000

Table 3 ^1H NMR acquisition parameters

These parameters were selected, by trial and error, to optimize the signal to noise ratio. 1000 transients were co-added for a total scan time of 1 hour 45 minutes per sample. After which there was no noticeable settling inside the sample tube. Throughout the study, the order in which samples analyzed was varied. The resulting FID's were Fourier transformed, with an exponential window function set to 0.3 Hz and phased using the NMR processing software MestReC (Ver. 4.9.9.9). The transformed spectra were then imported into Origin 8 in order to set a reference and for further analysis. The 0 ppm reference was set by recording the NMR spectra of a dilute solution containing 99.96% D_2O and ethanol. A shift of 0.152 ppm was required to set the CH_3 triplet to 1.17 ppm, according to the published data (Gotttlieb, Kotlyar, & Nudelman, 1997). This 0.152 ppm calibration shift was subsequently applied to all spectra acquired.

Chapter 3: Results

3.1 Optimization of Experimental Method

To obtain reproducible ^{1}H NMR spectra, several changes were made to the sample preparation procedure, treatment procedures, NMR parameters, and NMR sample tube washing technique. Due to the low concentration of biological sample material, several contamination related issues were solved over the course of this study. Signals arising from contamination tend to be easily detected as they are much larger in intensity, and have a much narrower line width when compared to the expected signal from living cells. Removing the high intensity contaminants prevents saturation of the spectra and enables a larger number of spectra to be co-added, leading to a higher sensitivity. By eliminating sources of contamination, the number of co-added spectra was increased from 100 to 1000 transients, resulting in an approximate 30 fold improvement in signal to noise. Acquiring 1000 transients required 1 hour 45 minutes per sample. The minimum number of samples per experiment was three (treated, untreated, and blank sample) requiring approximately six hours of instrument time. Increasing the number of scans beyond 1000 yielded little noticeable improvement compared to the increased time. Beyond 2 hours of acquisition time, the sample also began to settle leaving fewer bacteria in the acquisition region. The following is an outline of the more significant changes to the methodology used to increase the signal to noise in chronological order.

Due to the large number of samples to be run, it was decided that the ~$30 NMR sample tubes would be re-used instead of discarding after each use however, cleaning of these tubes was found to be a challenge from the onset. Typical methods of cleaning involve the use of organic solvents such as ethanol and acetone followed by thorough drying. The high sensitivity required to detect the small mass sample signal, made trace amounts of organic solvents show up strongly in the NMR spectra, thus limiting our ability to detect the organic molecules in the same sample. Figure 9 illustrates the results of early wash techniques, with the presence of ethanol triplet and quartet, at 1.18 ppm and 3.65 ppm respectively, and the acetone singlet at 2.22 ppm (Gotttlieb, Kotlyar, & Nudelman, 1997) seen after only 100 scans.

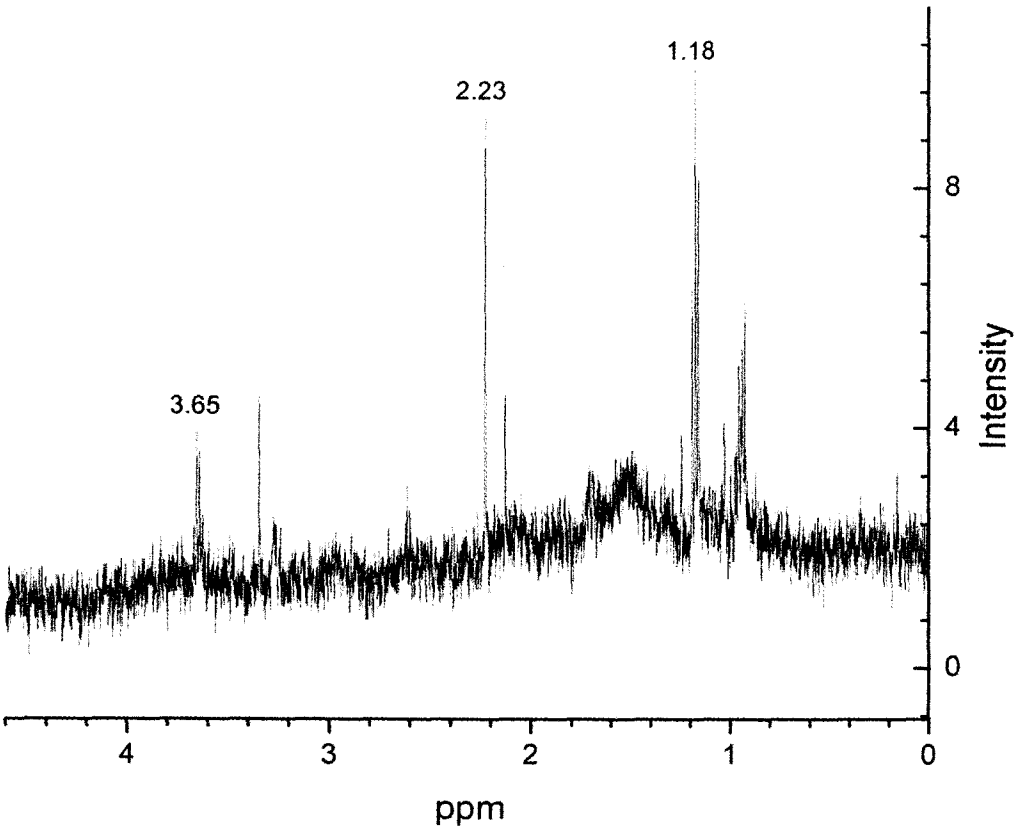

Figure 9 ^{1}H spectra of live *E. coli* cells suspended in 99.9% D_2O, 100 transients, ethanol and acetone peaks labeled

To eliminate the use of organic solvents, the sample tubes were cleaned using 9mm diameter pipe cleaner and regular dishwashing detergent. The tubes were washed then further rinsed with hot water to eliminate the detergent residue. The tubes were then rinsed with 1L of distilled water using an Aldrich NMR-Tube Cleaner (Z282391). After rinsing, the tubes were drained and placed in a 50^{O}C oven for 24 hours to dry. The resulting improvement to the blank D_2O spectra is illustrated (Figure 10)

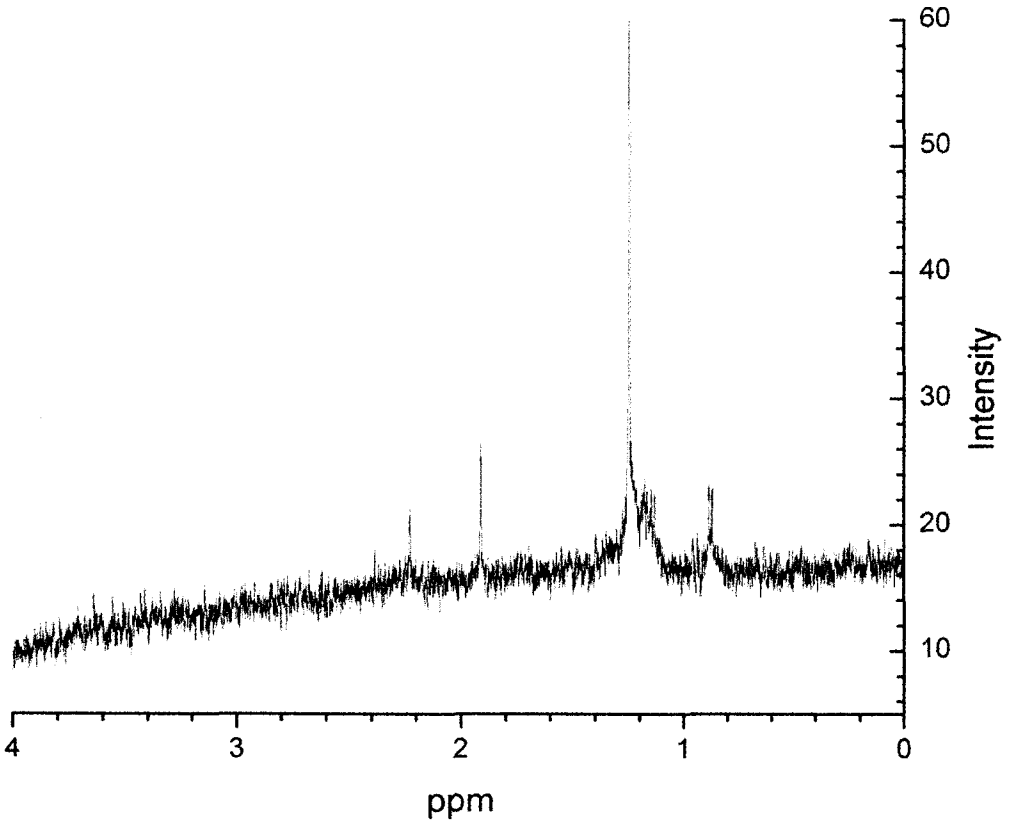

Figure 10 ^{1}H NMR spectra of 99.9% D_2O samples after improved washing techniques, 800 transients

Small signals present in the blank spectra (Figure 10) were thought to be due to contamination from the epoxy used in the construction of the sample holder, as well as airborne contaminants entering the sample during treatment. This was evident when we compared the spectra obtained from two blank samples that were placed in the sample holder and exposed to the atmosphere for 5 min (the standard treatment time). The exposure of two blank samples to the atmosphere introduced different contaminants into each sample with varying concentration. This can be seen in Figure 11 by noting the different peaks present, as well as their variation in intensity.

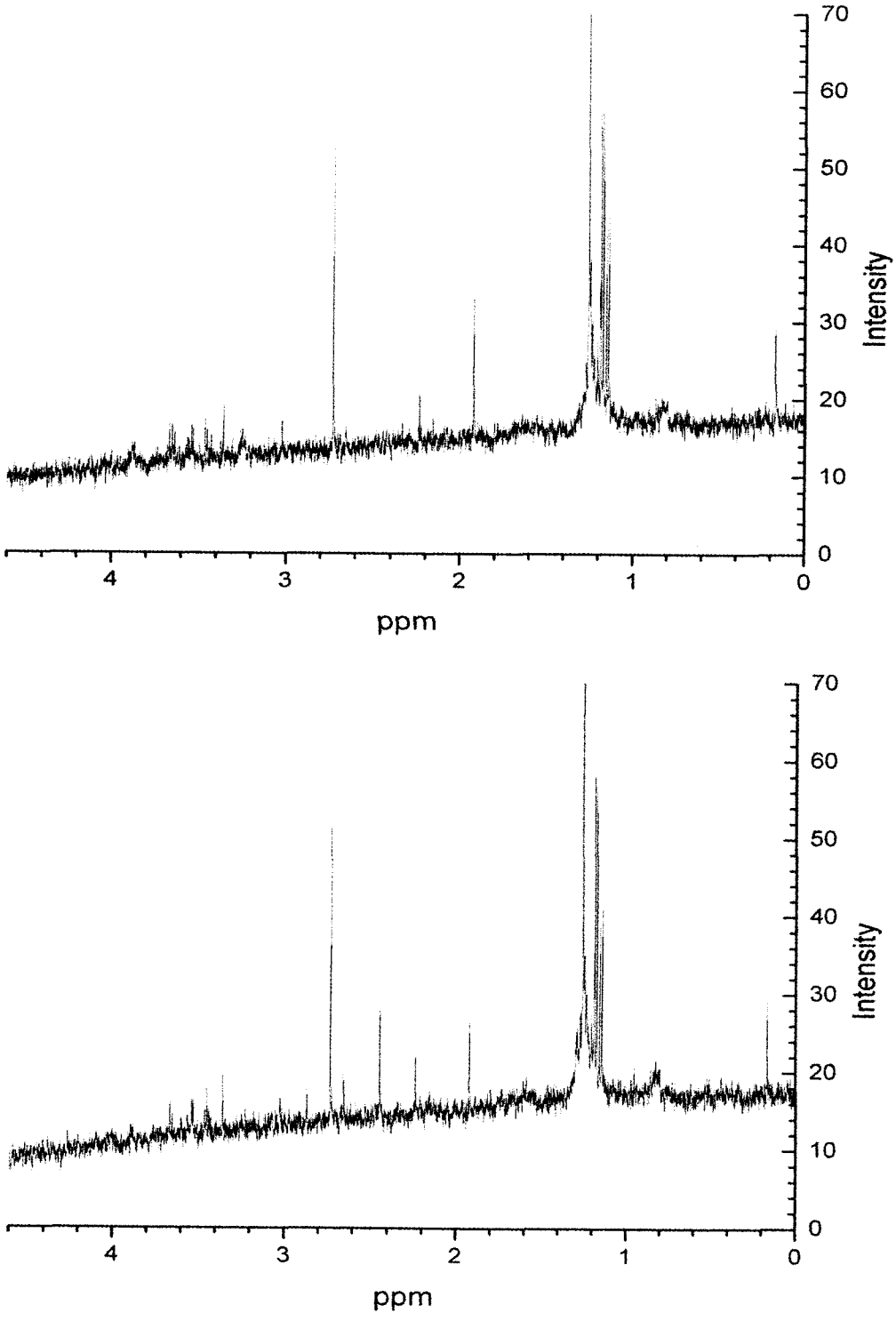

Figure 11 ^{1}H NMR spectra of two 99.9% D_2O samples placed into the sample holder for 5 minutes, 800 transients

Due to the lack of reproducibility seen in the blank spectra, construction of a new sample treatment chamber, illustrated in Figure 8, changed the sample container to an all glass vessel, eliminating the possibility of contamination from adhesives used previously. The new chamber was also sealable during treatment, eliminating the possibility of airborne contaminants from entering the sample. Purging the sealed sample chamber with 99.9% N_2 gas during treatment provided a positive pressure that eliminated both airborne particulates, as well as water vapor in the atmosphere from adsorbing into the sample. Implementing this sealed sample chamber greatly reduced contaminants illustrated in Figure 12 , however some unwanted and hard to identify peaks remained.

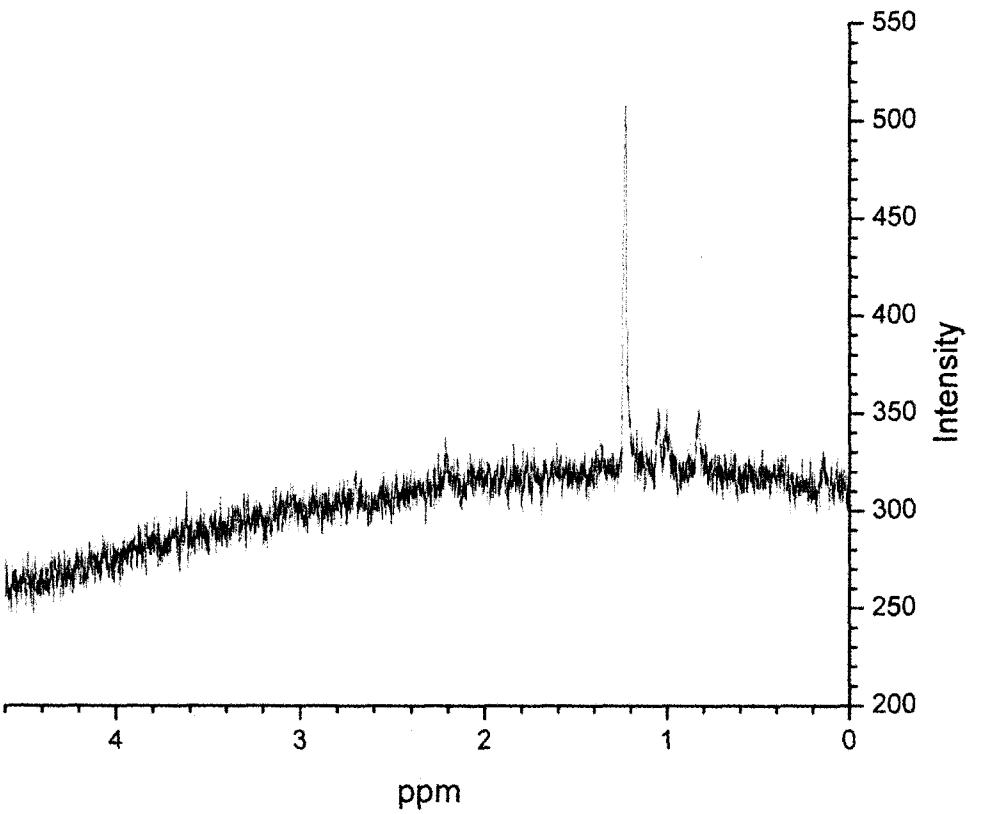

Figure 12 ^{1}H NMR spectra of 99.9% D_2O utilizing new sample holder, 800 transients

After further simplifying the growth and washing of the *E. coli* samples, impurities were discovered in the blank sample containing 99.9% D_2O. When the solvent was changed to the highest grade, 99.96% D_2O, impurity levels were below the detection limit. Figure 13 illustrates the full spectrum a blank sample. The broad H2O/DHO is seen from 4.8 to 5.4 ppm as well as

the portion of the spectra removed by the pre-saturation pulse at 4.81ppm. Figure 14 shows an expansion of the region of interest (0 to 4.8 ppm) and the absence of contaminant peaks.

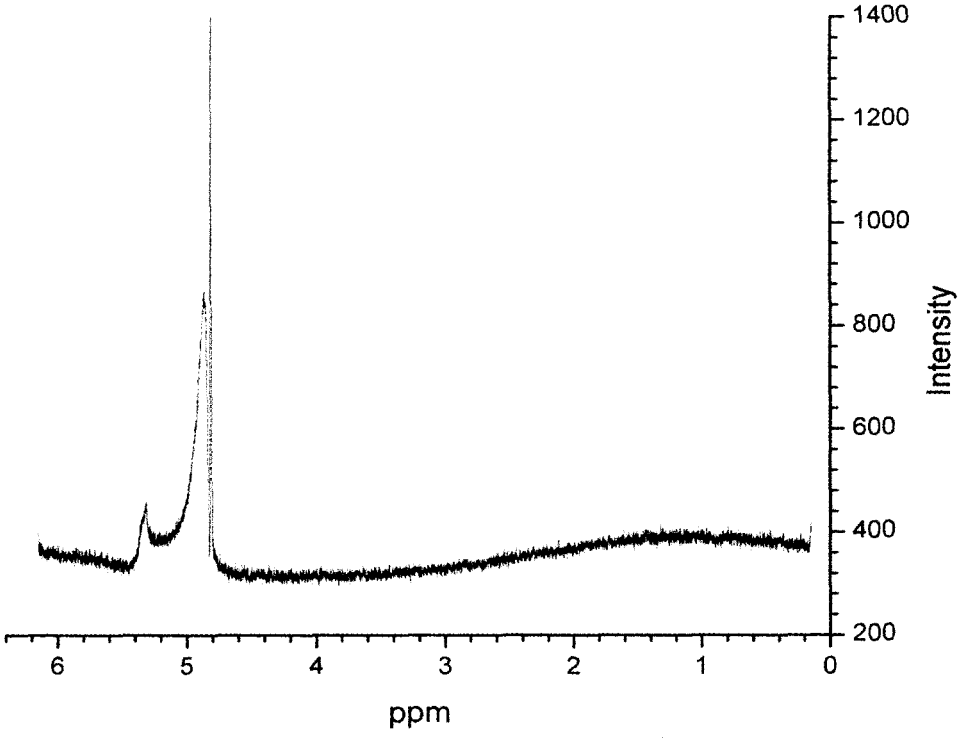

Figure 13 Full width ^{1}H NMR spectra of 99.96% D_2O, 1000 transients

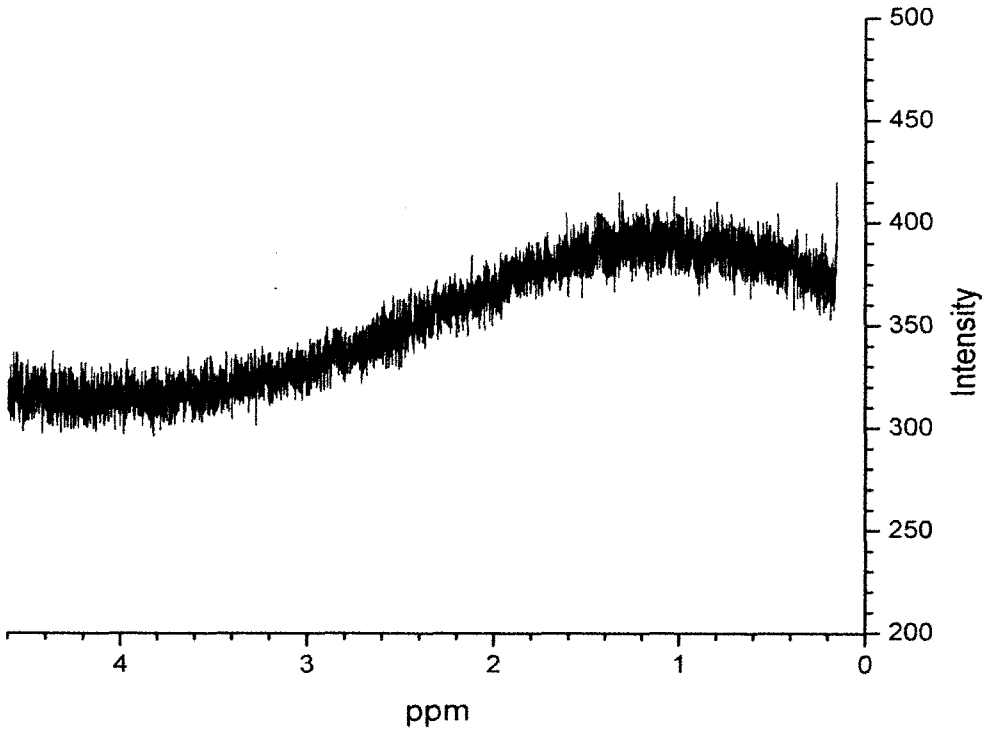

Figure 14 0 to 4.8 ppm region of Figure 11

The general rise in the signal amplitude in the low ppm range is an instrument effect that appears when the sensitivity range is highly expanded. It is visible in all spectra at sufficiently high y-axis expansion.

Further improvements in the overall signal-to-noise and reproducibility were realized after the NMR workstation software was replaced with the new Varian VNMRj software. This version introduced an automated shimming procedure that replaced the previously required manual tuning method. The operating parameters in the software were adjusted by trial and error to maximize sensitivity for a collection period of 1 to 2 hours, the time for which negligible settling would occur in the sample suspension. Since the new software had the ability to recall experimental operating parameters, a much improved experiment to experiment reproducibility was possible. This is particularly important for an instrument in a multi-user lab where dozens of different users may operate the machine between successive uses by one individual.

3.2 Drop Plate Assay Results

Using the bacteria culturing technique described in section 2.2.1, drop plate assays showed a consistent concentration of *E. coli* colony forming units (CFU) in untreated suspensions, for all samples. Concentrations of between 10^9 CFU/ml and 10^{10}CFU/ml were observed after an approximate 24 hour incubation in nutrient broth. Treatment and the re-culturing of a portion of the treated sample volume resulted in a decreased CFU concentration which varied between 10^3 and 10^6 CFU/ml. In all experiments, when comparing the untreated and treated CFU concentrations, a kill rate of over 99.9% was achieved. Figure 15 illustrates two Trypticase soy agar plates, onto which 5µl droplets of *E. coli* suspension were deposited. The numbers around the center indicate the number of 10x dilutions performed on the sample prior to deposition on the plates. Counting the number of colonies associated with a dilution number, enables the calculation of CFUs in the original sample volume.

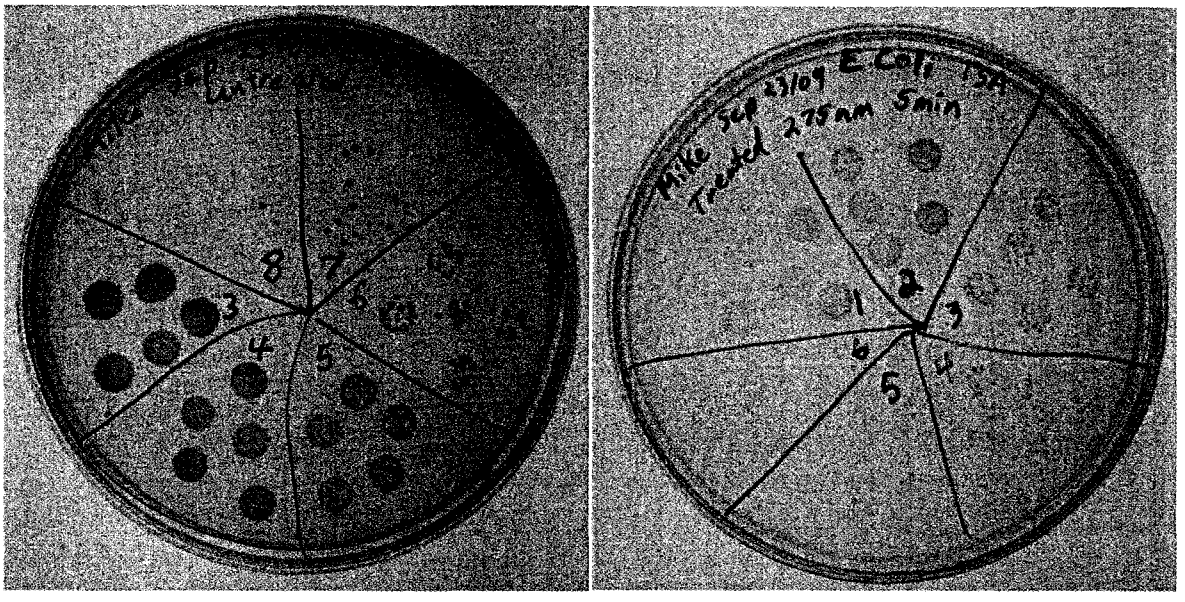

Figure 15 Drop plates after 12 hour incubation, (left) untreated sample colonies visible after 7, 10x dilution, (right) UV treated sample colonies visible after 4, 10x dilutions

All samples were slightly opaque due to the high concentrations of bacteria required for the NMR spectroscopy. The fluence of UV radiation delivered to the sample during treatment was approximately double that of the lethal dose reported for lower concentration suspensions used for calibrating the dose (Vermeulen, Keeler, Nandakumar, & Leung, 2007). A few bacteria

appear to be able to survive in the lower reaches of the treatment vessel because of partial shadowing of the radiation by bacterial absorption or scattering of the UV radiation in the upper layer of the sample suspension.

3.3 ^{1}H NMR Spectra

3.3.1 Untreated *E. Coli* Spectra

After optimization of the experimental methods and NMR acquisition parameters, reproducible spectra of live bacteria were obtained. A typical example of the spectrum obtained from live *E. coli* is illustrated in Figure 16. Although a pre-saturation pulse was applied, the most intense signal (4.8 to 5.2 ppm) still arises from H_2O, primarily from within the cell (~70% of the content of the bacteria cell) and HDO (Agris & Campbell, 1982). In the presence of H_2O, deuterium can exchange a deuteron with a hydrogen atom, resulting in a HDO molecule.

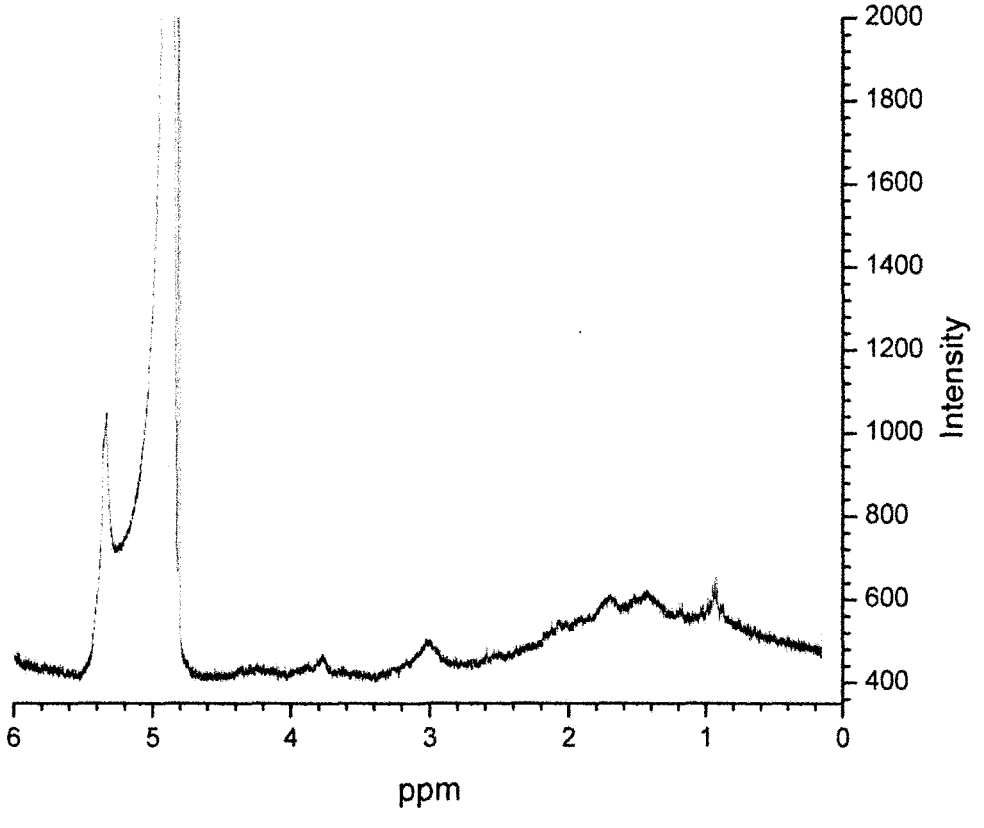

Figure 16 ^{1}H Spectra of live *E. coli* cells suspended in D_2O

No peaks were detected beyond the broad H_2O/HDO peak ending near 5.6ppm. Thus, the main region of interest lies between 0.5 and 4.7ppm. An expansion of this region, containing peak labels and peak envelopes is illustrated in Figure 17 and Figure 18.

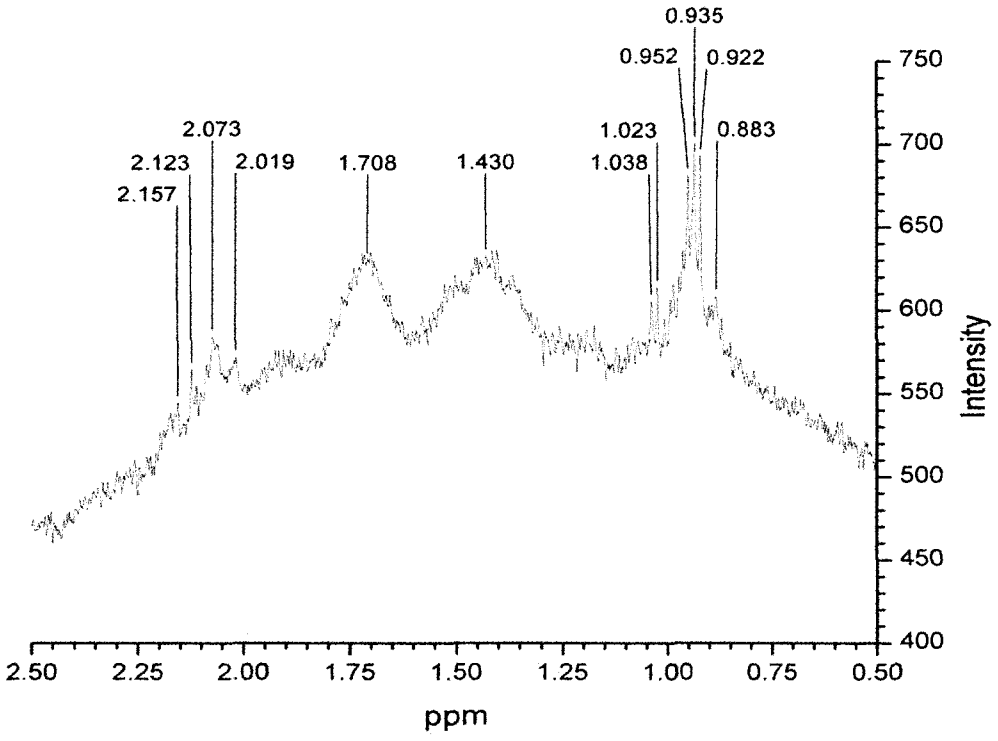

Figure 17 ^{1}H NMR spectra of live *E. coli*, 0.5 to 2.5 ppm region

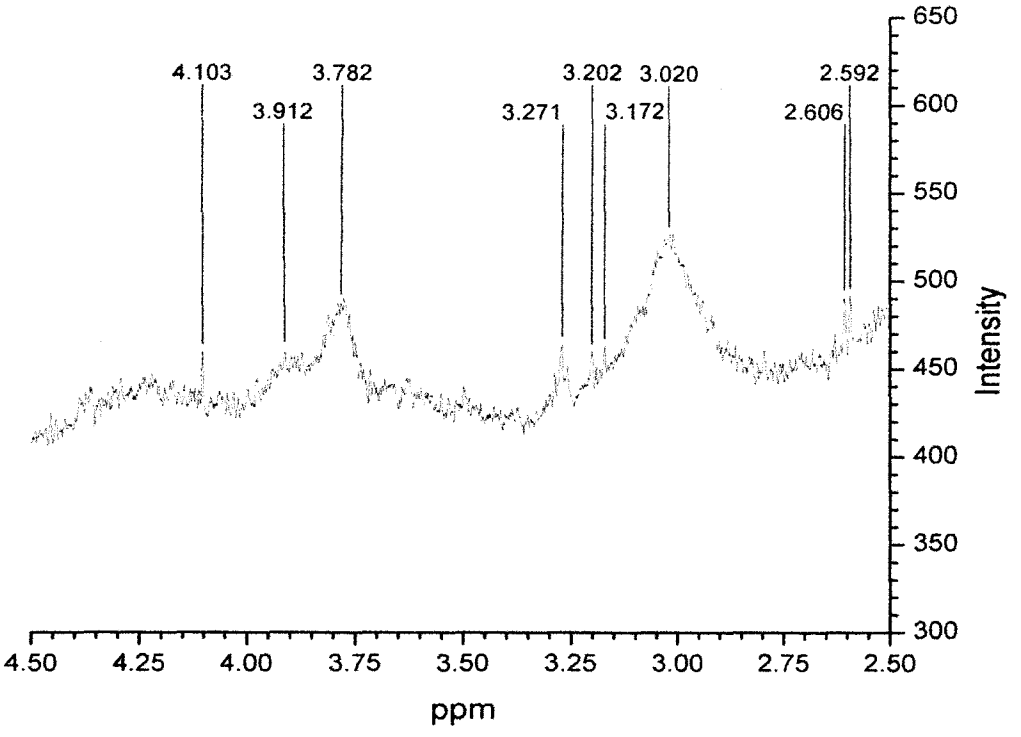

Figure 18 ^{1}H NMR spectra of live *E. coli*, 2.5 to 4.5ppm region

The spectrum of intact *E. coli* cells consists primarily of broad peak envelopes, centered at 1.430, 1.708, 3.020 and 3.78, all having an approximate width of 0.2 ppm. It is likely that a large number of unresolvable peaks are contained within these envelopes. The spectra also consist of a large number of narrower peaks at varying intensity.

3.3.2 UV Treated Spectra

Due to the relatively small treatment fluence delivered to the samples, it was expected that the ^{1}H NMR spectra of the treated samples would be very similar to the untreated samples. An example of the spectra obtained from treated *E. coli* is illustrated in Figure 19.

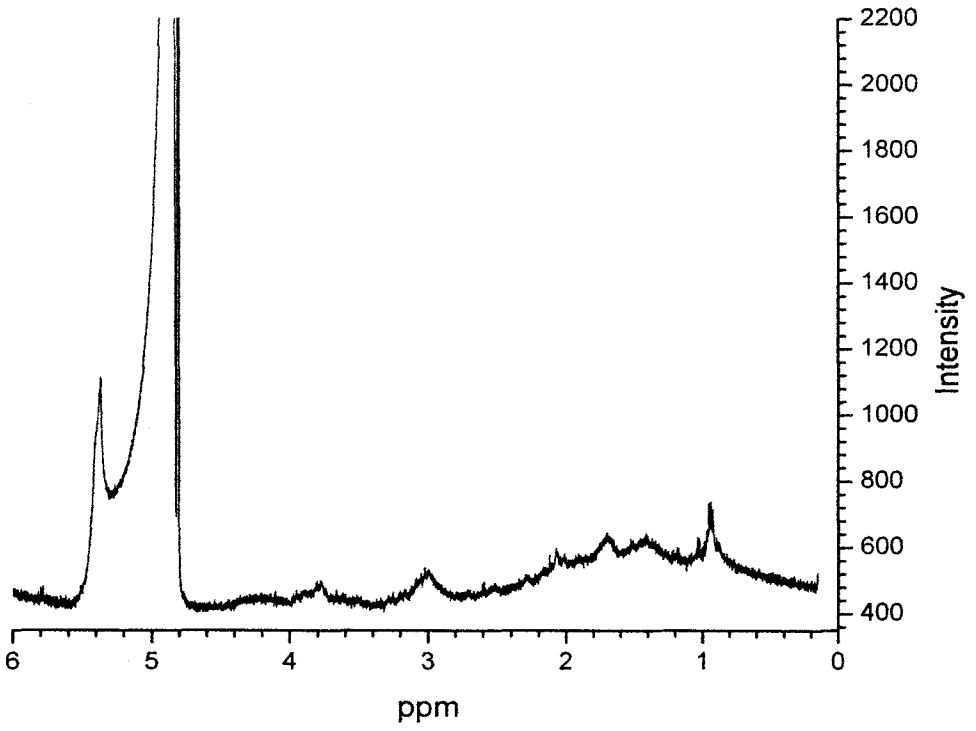

Figure 19 ^{1}H Spectra *E. coli* cell treated with a lethal dose of UV radation suspended in D_2O

As with the untreated spectra, the most intense signal, from residual H_2O and HDO, is located between 4.8 to 5.6 ppm and there were no peaks observed beyond 5.6 ppm. By overlaying spectra of a treated and untreated sample taken in succession, as is Figure 20 and Figure 21, the similarities and differences in the structure of the spectral features and the position of the peaks can be seen.

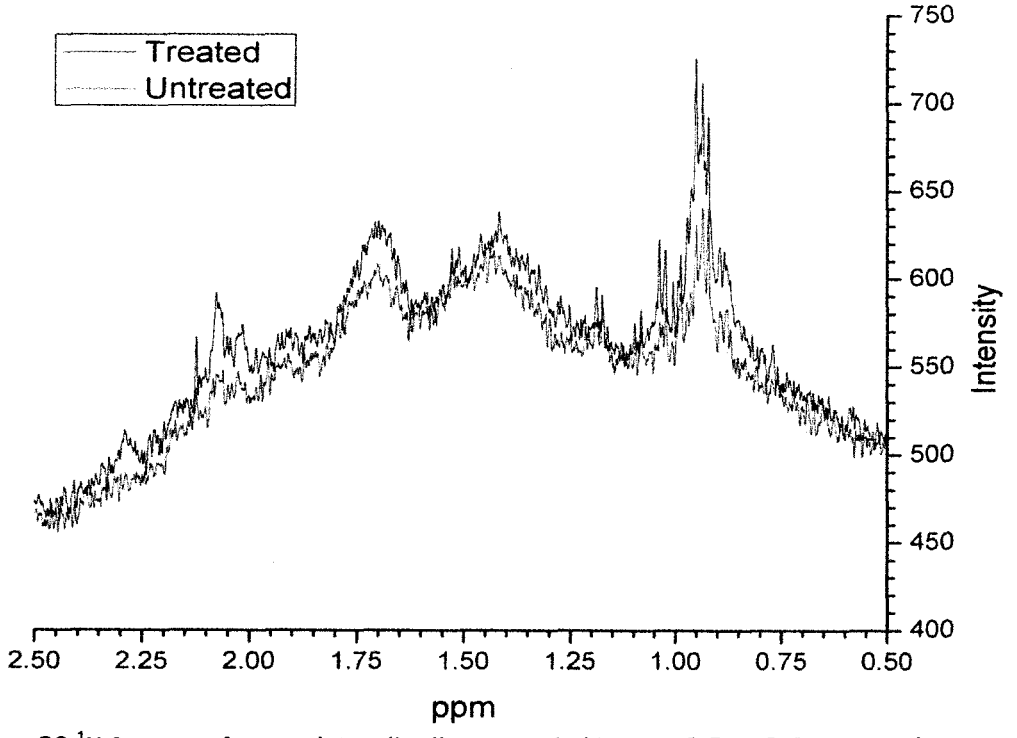

Figure 20 ^{1}H Spectra of treated *E. coli* cells suspended in D_2O, 0.5 to 2.5 ppm region

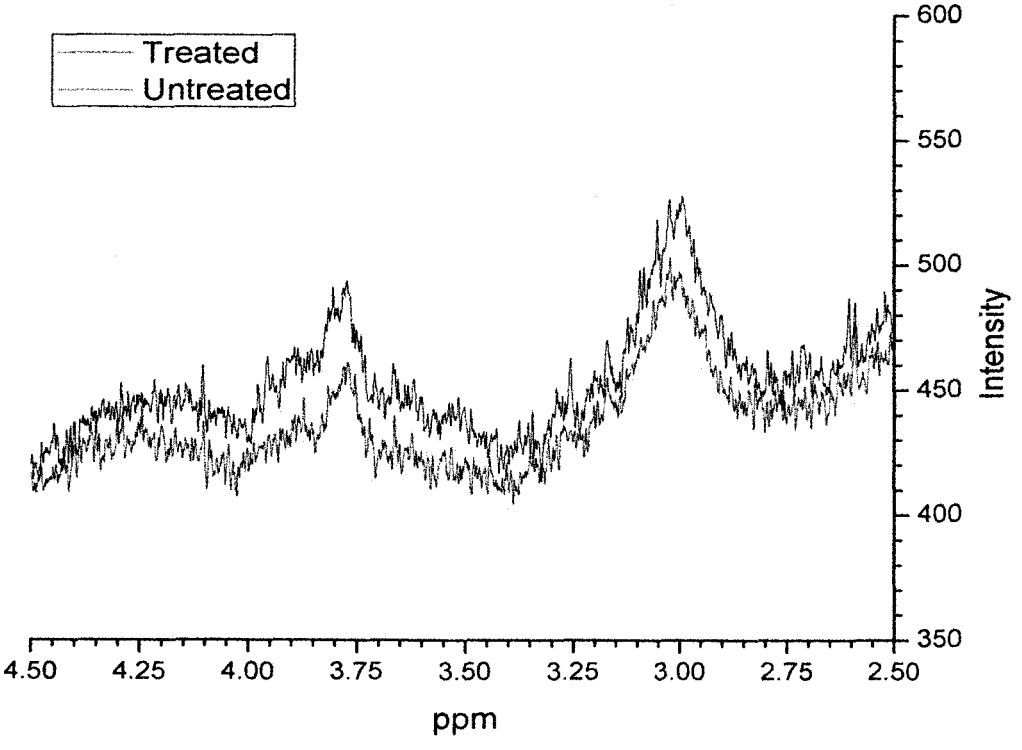

Figure 21 ^{1}H Spectra of treated *E. coli* cells, 2.5 to 4.5 ppm region

While the spectra of the treated and untreated spectra seem similar, much of the treated spectra are of a higher intensity than the untreated spectra. There are also subtle variations in the intensity of the labeled peaks. To further evaluate the change in peak intensity, the difference between the untreated and treated spectra was calculated. While several dozen of treated and untreated sample spectra were taken over the course of this study, the last three experiments, nine spectra in total, were of the highest quality. Hence, these final three spectra were used to produce both the difference and ratio spectra. The resulting spectra are noisy, as would be expected, since changes in the sample resulting from a short exposure to light will be subtle. However, it was observed that the individual difference and ratio spectra have very reproducible major and minor peaks, making it possible to co-add several of them together to provide an aggregate averaged result. After averaging, a Savitsky-Golay FFT smoothing was applied to the spectra with parameters listed in Table 4. The final resulting difference spectrum along with peak selection is illustrated in Figure 22 and Figure 23.

Points of Window	Boundary Conditions	Polynomial Order
40	None	2

Table 4 Savitzky-Golay Smoothing Parameters

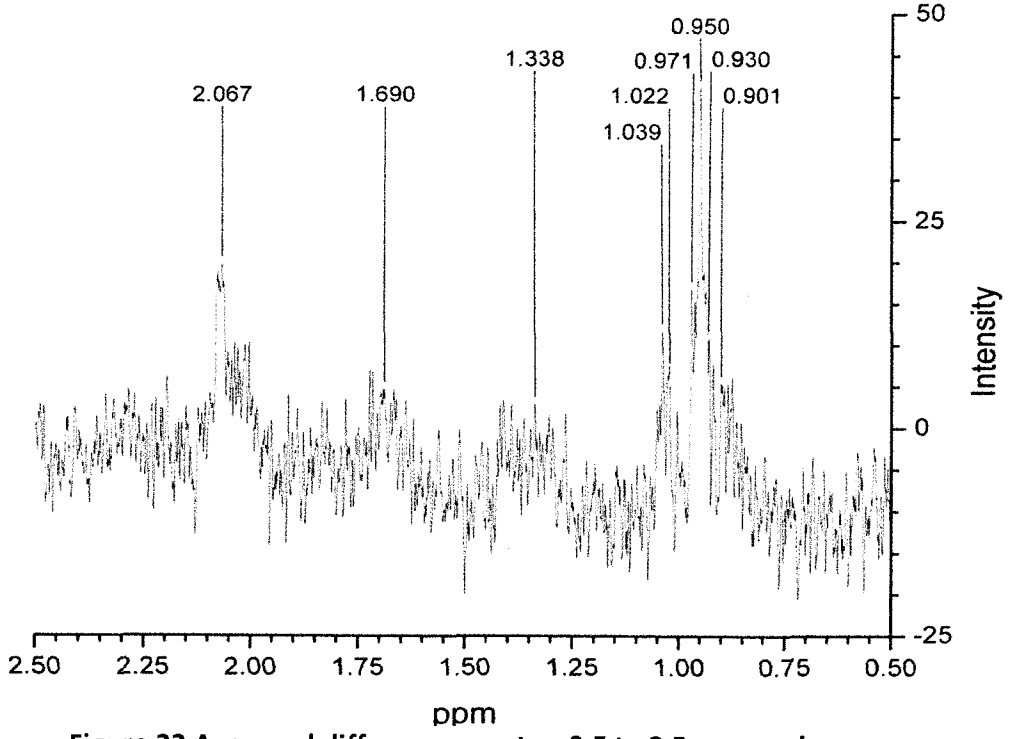

Figure 22 Averaged difference spectra, 0.5 to 2.5 ppm region

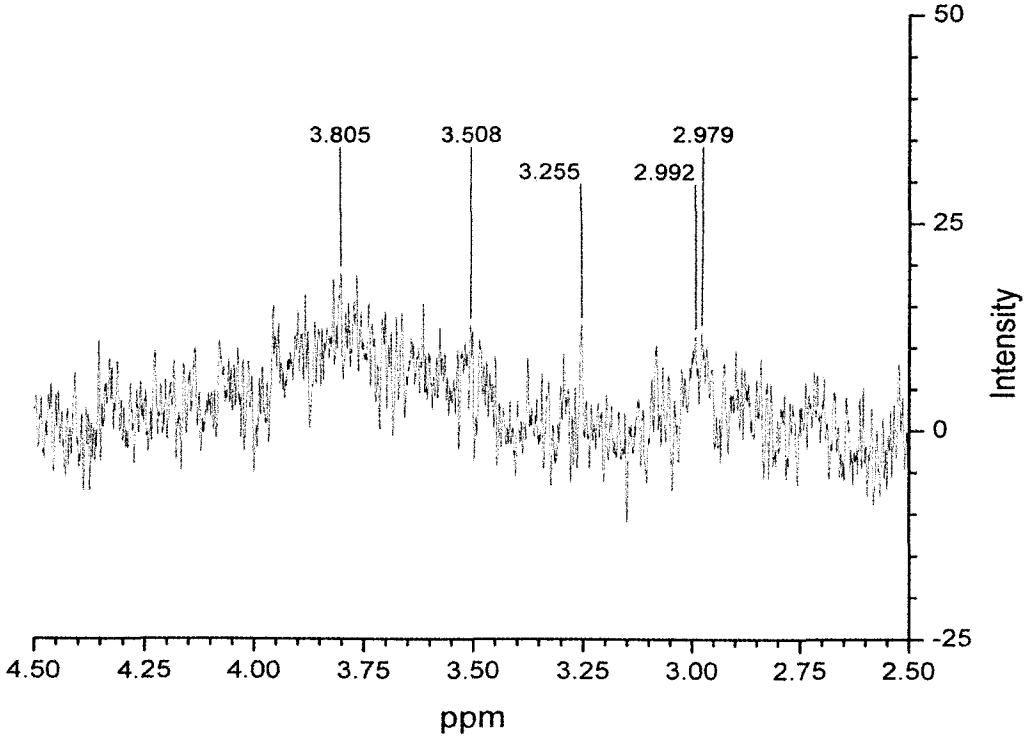

Figure 23 Averaged difference spectra, 2.5 to 4.5 ppm region

The changes in the difference spectrum are attributed to the UV treatment delivered to the sample. Furthermore, because of the small changes in the spectral peak intensities and positions, the ratio of the treated to untreated spectra displayed the changes in fractional percentages directly.

3.3.3 Spectra Analysis and Peak Identification

In an attempt to identify the biological molecules responsible for all of the peaks, the freely accessible and publicly maintained Biological Magnetic Resonance Data Bank (BMRB) has proven to be an extremely valuable source for ^{1}H NMR reference spectra. This data bank is maintained by the University of Wisconsin at Madison, and 'hosts a collection of NMR data for small biomolecules of metabolic interest'. The database can be searched by compound name or by peak position (including linewidth, and intensity). The accuracy of the spectra in this bank is the 'responsibility of the depositors' and as such, published peak information (Govindaraju, Young, & Maudsley, 2000), (Agris & Campbell, 1982) was also used. Since no uncertainties in peak positions are given in the data bank, the uncertainty in the ppm comparisons can only be estimated for the data collected in this project. From the data collection and analysis experienced in this study, the uncertainty in the ppm location of a given peak was mainly determined by the purity (linewidths) of the calibrating reference samples. We assign an uncertainty of ± 0.015 ppm for the x-axis location of the individual spectra collected during these experiments, based on several calibration runs. The precision of the ppm axis is perhaps a factor of ten higher than this accuracy however. Thus, it is reasonable to assume that in comparing data in this project to that of the BMRB data base, and published data, that an uncertainty in peak positions in the comparison of ± 0.020 ppm would be reasonable.

An overlay of untreated *E. coli* spectra with the averaged difference spectra is illustrated in Figure 24. Although the y-axis scale is not consistent between the two spectra, this figure serves as a visual indicator of which peaks were affected due to the UV treatment. It is interesting to note that there are peaks which appear in the difference spectra that appear to be absent from the whole cell spectra, for example, at 2.06 ppm. This could indicate that there

are multiple compounds responsible for the whole cells spectra, while only the compound contributing to the peak at 2.06 ppm are being affected by UV treatment.

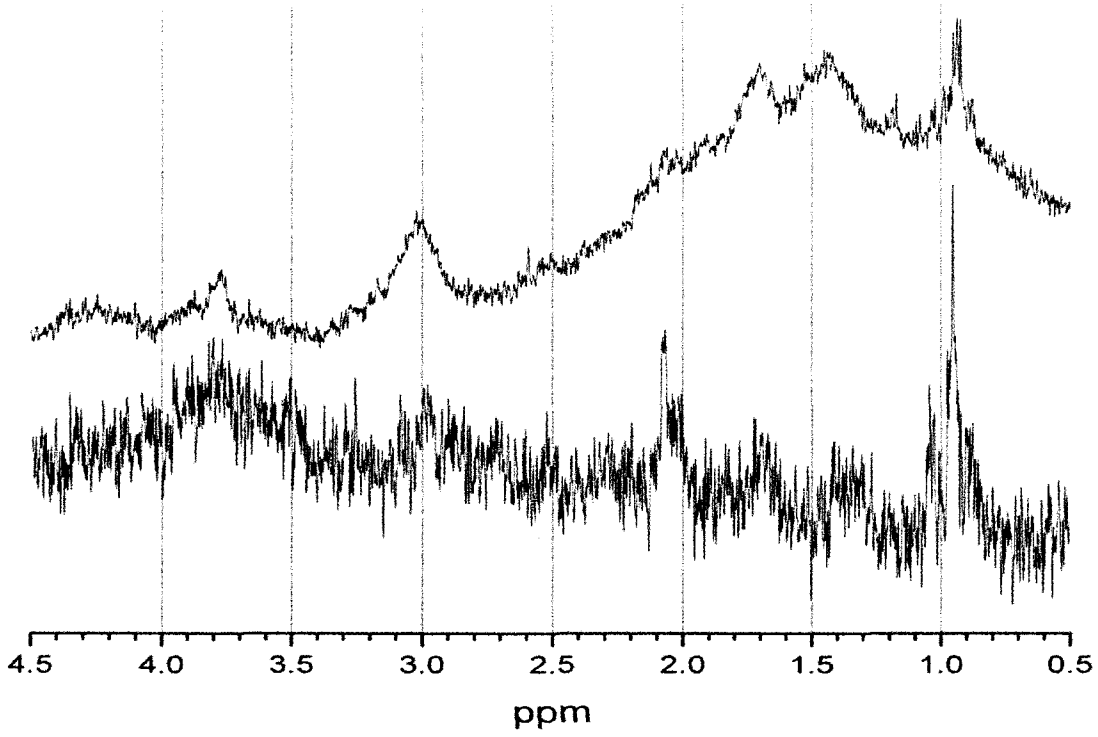

Figure 24 (upper) Untreated *E. coli* spectra, (lower) averaged difference spectra

Recalling the major molecular components in the bacterium as given in Table 1, one might expect peaks to be caused mainly by proteins, DNA-RNA, and membranes. Since the proteins are first formed from the amino acids with subsequent bonding to simple or complex sugars, these sub-groups may also be visible. To determine the possible constituents of the spectra a search using the BMRB, and published literature was conducted to identify possible candidate compounds using the peaks identified in the *E.coli* spectra and the difference spectra. Once candidate compounds were identified the spectra, peak position, and relative intensity, was compared to the sample spectra. A comparison of amino acid spectra with untreated *E. coli* is illustrated in Figure 25 with the peak positions of the amino acids listed in Table 5.

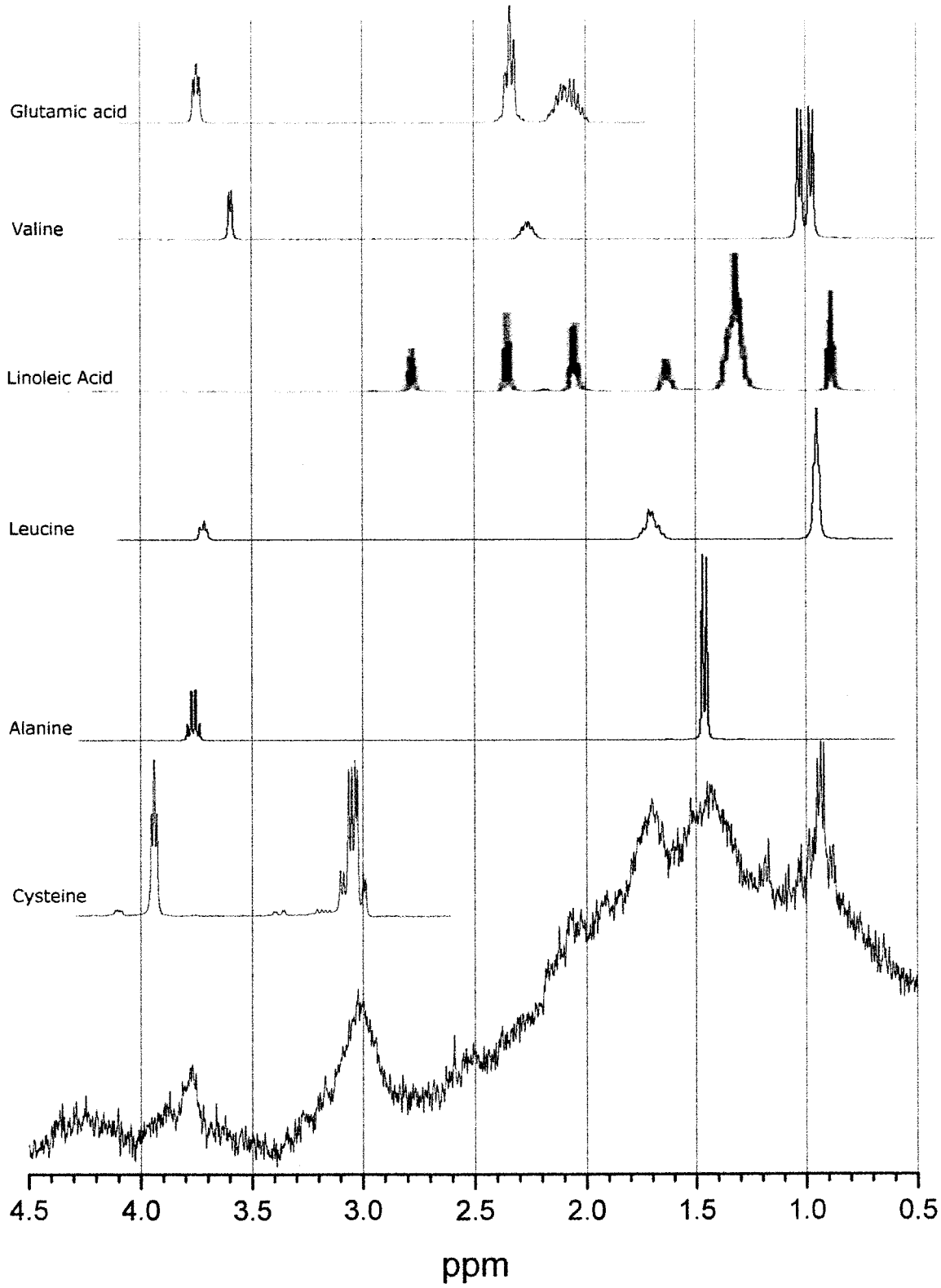

Figure 25 Untreated ^{1}H spectra of untreated *E. coli* with spectra of select biomolecules

Molecule	Peak Location (ppm)	Possible Sample Peak position (ppm)
Cysteine	3.04, 3.94	3.020(e), 3.912
Alanine	1.466, 3.767	1.411, 3.782(e)
Leucine	0.949, 1.714, 3.722	0.952, 1.708(e), 3.782(e)
Linoleic Acid	0.89, 1.319, 2.049, 2.771	0.883, 1.430(e), 2.073, (NP)
Valine	0.977, 1.029, 2.262, 3.594	0.972, 1.023, (NP), (NP)
Glutamic Acid	2.07, 2.338, 3.745	2.073, (NP), 3.782(e)

Table 5 Chemical shifts for amino acid groups in Figure 25, (NP) – no peaks present in acquired spectra, (e) – peak envelope with a width of approximately ±0.2 ppm

As multiples are not resolved in the raw spectra, it is difficult to unequivocally determine the exact compounds contributing to the spectra. Of all the amino acids, the spectra of glutamine, alanine, leucine and valine appear to be the closest match to the acquired spectra. Peaks located around 1 ppm may also be the result of lipid components including the methyl ($-CH_3$) group which is located at 0.9 ppm (Mikhailenko, Philchenkov, & P, 2005).

As noted in section 3.3.2, changes in the treated and untreated spectra were mainly seen in the varying intensity of the detected peaks. Because it is impossible to determine if a specific peak is the result of one compound or is the sum of multiple compounds, the change in intensity observed in one peak of the treated samples could be the result of a number of compounds. By subtracting the spectral data of the treated samples from the untreated samples, acquired on the same day, we obtain the spectra, seen in Figure 26, of those peaks whose intensity has been altered by the UV treatment.

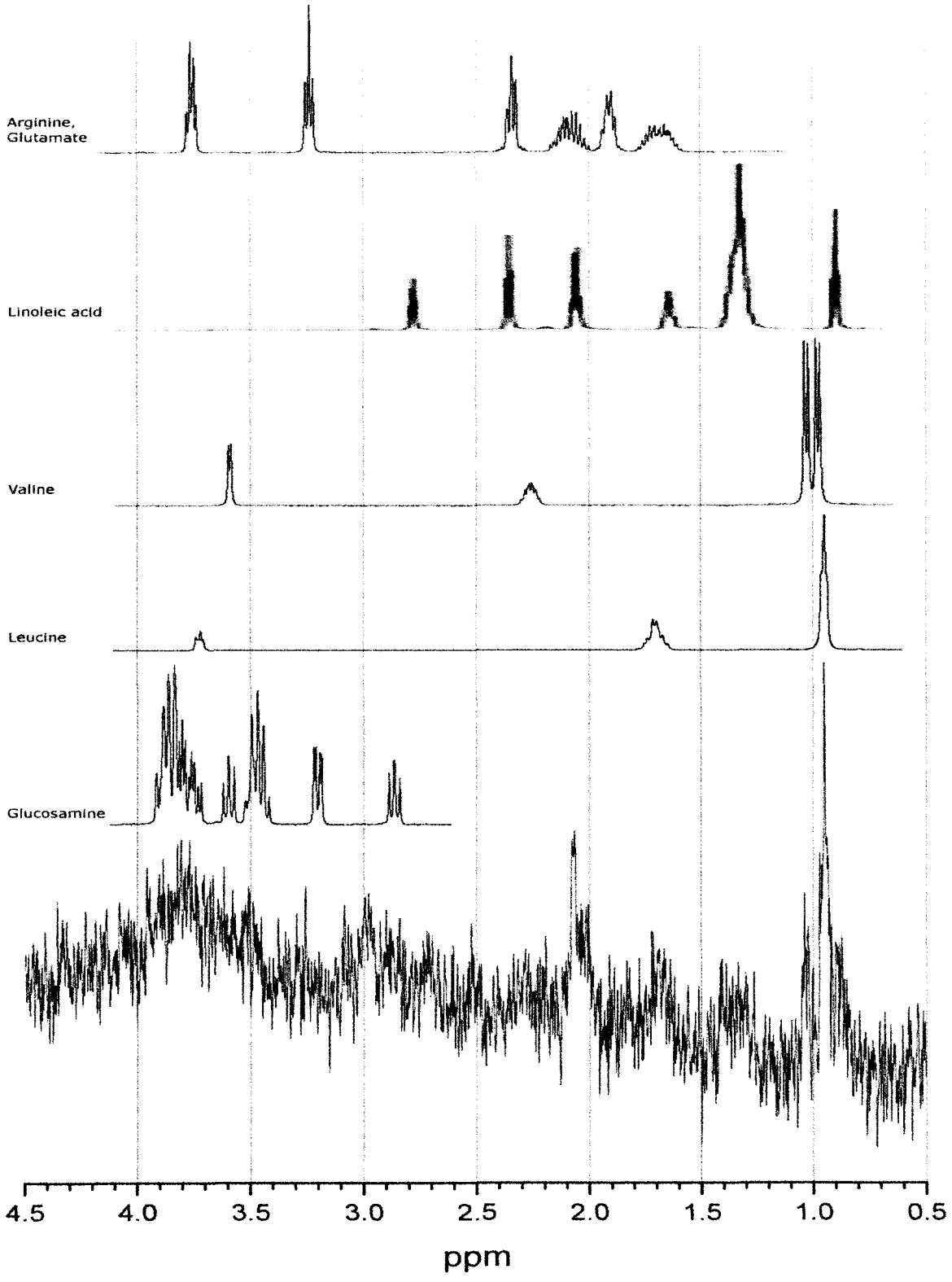

Figure 26 Averaged Difference spectra of *E. coli* with spectra of select biomolecules

Molecule	Peak Location (ppm)	Possible Sample Peak position (ppm)
Leucine	0.949, 1.714, 3.722	0.950, 1.717, 3.805
Valine	0.977, 1.029, 2.262, 3.594	0.971, 1.022, (NP), 3.508
Linoleic Acid	0.89, 1.319, 2.049,2.347 2.771	0.883, 1.430, 2.073, (NP)
Arginine, Glutamate	1.684, 1.905, 2.079, 2.34, 3.233, 3.75, 3.7633	1.690, 2.06(e), 2.06(e), (NP), 3.255, 3.805(e), 3.805(e)

Table 6 Chemical shifts for amino acid groups in Figure 26, (NP) – no peaks present in acquired spectra, (e) – peak envelope with a width of approximately ±0.2 ppm

3.3.3.1 Ratio Spectra vs. Difference Spectra

The difference spectrum and a ratio of the two raw spectra (treated/untreated) show virtually identical peak positions due to sample treatment. To see the magnitude of the relative effects, a cursory examination shows that, if the two spectra are almost the same, with small signals on each (ignoring noise), then the two raw spectra can be represented as $S + dS_1$ and $S + dS_2$ with difference $dS_1 - dS_2$. The relative change would be $(dS_1 - dS_2)/S$. The mathematics for this manipulation of the spectra requires two uses of the noise components which will add in general. If, on the other hand, the ratio of the two spectra is taken, with dS_1 and $dS_2 << S$

$$\frac{S + dS_1}{S + dS_2} = \frac{S\left(1 + \frac{dS_1}{S}\right)}{S\left(1 + \frac{dS_2}{S}\right)} = \left(1 + \frac{dS_1}{S}\right)\left(1 + \frac{dS_2}{S}\right)^{-1}$$

On using a binomial expansion

$$= \left(1 + \frac{dS_1}{S}\right)\left(1 - \frac{dS_2}{S} + \ldots\right)$$

for small dS's. Multiplying through and collecting gives

$$= 1 + \frac{dS_1}{S} - \frac{dS_2}{S} + \cdots = 1 + \frac{dS_1 - dS_2}{S}$$

plus higher terms in $dS_1\, dS_2$. This result provides the relative change with respect to 1 in one mathematical manipulation of the data with its noise. As shown in Figure 26, the y-axis of the treated to untreated spectra quantifies relative change in peak amplitude due to sample treatment.

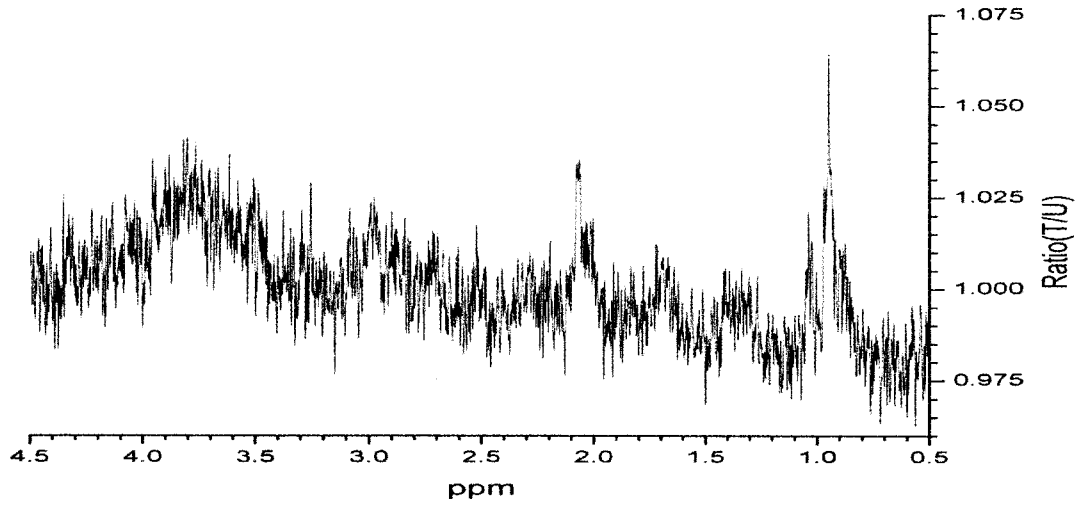

Figure 27 Ratio spectrum of treated to untreated samples with the y-axis exhibiting relative change in intensity due to UV treatment

3.4 Discussion

All of the peaks in the difference and ratio spectra are positive going peaks. Although the baseline for the ratio spectrum is slightly below unity at 0 ppm, and increasing slowly with increasing chemical shift numbers, there are no clearly identifiable negative going peaks caused by the UV treatment of the samples. Since the peaks represent component enhancements in some way or another, it is interesting to attempt to identify their possible origins.

From examination of Figure 26 and component spectra from the BMBR database, it appears that the difference spectral peak enhancements occur at chemical shift positions characteristic of free components of sugars compounds, amino acids, and lipids. There is a significant increase in the difference spectrum amplitude in the sugars portion of the spectrum lying between about 3.4 and 4.0 ppm. While there is little evidence to suggest direct enhancements due to nucleic acid side chains in any of the spectra, the phosphate-sugar backbone in both the DNA and RNA molecules could be adding to that of other sugar/saccharide components after treatment by the UV. Other nucleic and DNA/RNA enhancements might occur in the H_2O and HDO peak region. However, no reproducible, resolvable peaks could be obtained in this region.

The free amino acid peaks appear to be the most common new component peaks and can be expected to occur as a result of the protein de-composition process (Ingraham, Maaloe, & Neidhardt, 1983). One possible cause of the apparent production of 'free amino acids' is the bond breaking capability of the high energy UV photons. In addition, radicals produced by this bond breaking action may lead to other reaction pathways. A major reactive channel can be described by the following cyclic model.

3.4.1 Possible effects due to Reactive Oxygen Species (ROS)

In the presence of reactive oxygen species such as OH^- which are readily produced by the 275nm bond breaking photons used in this study, the lipid peroxydation chain reaction can be initiated (Farr & Kogoma, 1991). This process proceeds by a free radical chain reaction mechanism. It most often affects polyunsaturated fatty acids, because they contain multiple double bonds in between the methylene -CH2- groups that possess especially reactive hydrogen atoms (Halliwell & Chirico, 1993). As with any radical reaction the reaction consists of three major steps: initiation, propagation and termination.

Initiation: is the step whereby a fatty acid radical is produced. The initiators in living cells are most notably reactive oxygen species (ROS), such as OH^- , which combines with a hydrogen atom to make water and a fatty acid radical.

Propagation: The fatty acid radical is not a very stable molecule so it reacts readily with molecular oxygen, thereby creating a peroxyl-fatty acid radical. This too is an unstable species that reacts with another free fatty acid producing a different fatty acid radical and a lipid peroxide or a cyclic peroxide if it had reacted with itself. This cycle continues as the new fatty acid radical reacts in the same way.

Termination: When a radical reacts with a non-radical it always produces another radical, which is why the process is called a "chain reaction mechanism." The radical reaction stops when two radicals react and produce a non-radical species. This happens only when the concentration of radical species is high enough for there to be a high probability of two radicals actually colliding. The reaction can also be terminated if the radical reacts with an antioxidant species.

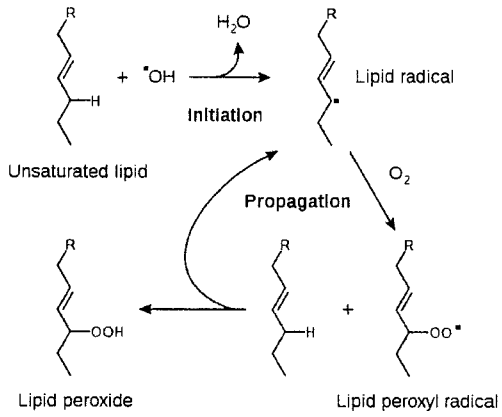

Figure 28 Lipid peroxidation chain reaction

Before termination of this reaction, there is likely to be major damage to the cell membrane, which consists mainly of lipids. Moreover, the free radicals will be mobile enough to react with other components in the bacterial cell, including the proteins and other cell constituents. The essentially free fragments produced by this type of chain reaction may be the cause of the greater part of the changes observed between the treated and untreated sample spectra.

In summary protein decomposition appears to produce new or at least enhanced free amino acid peaks in the NMR spectra. The sizable increase in the sugar region of the spectrum could be related to DNA/RNA backbone or other polysaccharide related fragments. The lipid spectral region is also enhanced by the treatment. It is worth emphasizing however that the component spectra chosen to fit the experimental data do not represent an exhaustive search and other compounds may also contribute significantly to the analysis. At this stage, the three groups of compounds described in this report appear to play the major role in explaining the observed results.

3.5 Conclusion

E.coli has been successfully cultured and used as a sample for a ^{1}H NMR investigation of the effects caused by a lethal fluence of UV light for the first time to our knowledge. Once sample preparation, treatment, and NMR mounting methods were optimized, the high sensitivity, high resolution capabilities of the 500 MHz Varian Unity Innova NMR spectrometer produced reproducible results for a series of experiments. These results reveal significant changes to the ^{1}H NMR spectra after differencing the treated and untreated *E.coli* samples when the treated samples were exposed to 275nm light in excess of the known lethal fluence. Increases in peak intensities of 4-8% are observed in the 0.8-1.1 ppm chemical shift region, which is characteristic of lipids, and the amino acids leucine and valine. Increases of approximately 3.5-4% appear near the arginine and glutamine 2 ppm peak location, and in the 3.4-4 ppm region characteristic of various sugars and possibly some amino acids. The remaining increase in peak intensity of 1.5-2.5% seems mainly due to amino acids and lipid components. Since photons at 275nm wavelength have enough energy to break all of the principle bonds in an organic molecule, the apparent partial fragmentation of much of the bacterial mass into smaller molecular components may not be too surprising. The difference spectrum appears to be well fitted by component spectra from various amino acids, sugar groups and membrane/lipid groups.

Further investigations appear to be warranted now that a successful overall method has been established. Experiments carried out at higher net photon fluences should increase the signal to noise ratio. Also, the use of photons of lower energy (longer wavelength) that would break only a sub-set of the organic bonds might reveal different spectral changes in the ratio spectrum due to the treatment.

References

Agris, P., & Campbell, I. (1982). Proton nuclear magnetic resonance of intact friend leukrmia cells: phosphorylcholine increase during differentiation. *Science , 216*, 1325-1327.

Alberts, B., Johnson, A., Lewis, J., Raff, M., Roberts, K., & Walter, P. (2008). *Molecular Biology of the Cell.* New York: Garland Science, Taylor & Francis Group, LLC.

Ames, G. F. (1968). Lipids of Salmonella typhimurium and Escherichia coli: Structure and Metabolism. *Journal of Bacteriology , 95*, 833-843.

Ananthaswamy, H. N., & Eisenstark, A. (1977). Repair of hydrogen peroxide-induced single-strand breaks in Escherichia coli deoxyribonucleic acid. *Journal of Bacteriology , 130* (1), 187-191.

Balci, M. (2005). *Basic 1H-13C- NMR Spectoscopy.* Amsterdam, The Netherlands: Elsevier B. V.

Betancourt, W. Q., & Rose, J. B. (2004). Drinking Water Treatment Processes for Removal of Cryptosporidium and Giardia. *Veterinary Parasitology , 126*, 219-234.

Betts, G. D. (2000). Controlling E. coli 0157. *Nutrition and Food Science , 30* (4), 183-186.

Brauer, M. (2003). In vivo monitoring of apoptosis. *Progress in Neuro-Psychopharmacology & Biological Psychiatry , 27*, 323-331.

Burger, A., Raymer, J., & Bockrath, R. (2002). DNA damage-processing in E. coli: on-going protein synthesis is required for fixation of UV-induced lethality and mutation. *DNA Repair , 1*, 821-831.

Cavalcante, A. K., Martinez, G. R., Mascio, P. D., Menck, C. F., & Agnez-Lima, L. F. (2002). Cytotoxicity and mutagenesis induced by singlet oxygen in wild type and DNA repair deficient Escherichia coli strain. *DNA Repair , 1*, 1051-1056.

Chamberlain, J., & Moss, S. H. (1987). Lipid peroxidation and other membrane damage produced in escherichia coli K1060 by near-UV radiation and deuterium oxide. *Photochemsitry and Photobiology , 45* (5), 625-630.

Chang, J. C., Ossoff, S. F., Lobe, D. C., Dorfman, M. H., Dumais, C. M., Qualls, R. G., et al. (1985). UV Inactivation of Pathogenic and Indicator Microorganisms. *Applied and Environmental Microbiology , 49* (6), 1361-1365.

Chary, K. V., & Govil, G. (2008). *NMR in Biological Systems.* Dordrecht, The Netherlands: Springer.

Cooper, W. A., Bartier, W. A., Rideout, D. C., & Deelikatny, E. J. (2001). 1H NMR Visible Lipids are Induced by Phosphonium Salts and 5-Fluorouracil in Human Breast Cancer Cells. *Magnetic Resonance in Medicine , 45*, 1001-1010.

Farr, S. B., & Kogoma, T. (1991). Oxidative stress responses in Escherichia coli and Salmonella typhimurium. *Microbiological Reviews , 55* (4), 561-585.

Gotttlieb, H. E., Kotlyar, V., & Nudelman, A. (1997). NMR chemical shifts of common laboratory solvents as trace impurities. *The Journal of Organic Chemistry , 62*, 7512-7515.

Govindaraju, V., Young, K., & Maudsley, A. (2000). Proton NMR chemical shifts and coupling constants for brain metabolites. *NMR in Biomedicine , 13*, 129-153.

Grivet, J. P. (2001). NMR and Miccroorganisms. *Current Issues in Molecular Biology , 3* (1), 7-14.

Hakumaki, J. M., & Kauppinen, R. A. (2000). 1H NMR visible lipids in the life and death of cells. *Trends in Biochemical Sciences , 25*, 357-362.

Halliwell, B., & Chirico, S. (1993). Lipid peroxidation: its mechanism, measurement, and significance. *The American Journal of Clinical Nutrition , 57*, 715S-725S.

Hijnen, W. A., Beerendonk, E. F., & Medema, G. J. (2006). Inactivation credit of UV Radiation for Viruses, Bacteria, and Protozoan (oo)cysts in Water: A Review. *Water Research , 40*, 3-22.

Hockberger, P. E. (2002). A History of Ultraviolet Photobiology for Humans, Animals and Microorganisms. *Photochemistry and Photobiology , 76* (6), 561-579.

Hollaender, A. (1943). Effects of Long Ultraviolet and Short Visible Radiation (3500 to 4900A) on Escherichia Coli. *Journal of Bacteriology , 46* (6), 531-541.

Holmes, K. T., Williams, P. G., May, G. L., Gregory, P., Wright, L. G., Dyne, M., et al. (1986). Cell surface involvment in cancer metastasis: an NMR study. *Federation of European Biochemical Societies , 202* (1), 122-126.

Ingraham, J. L., Maaloe, O., & Neidhardt, F. C. (1983). *Growth of the Bacterial Cell.* Sunderland: Sinauer Associates, Inc.

Jagger, J. (1967). *Introduction to Research in Untraviolet Photobiology.* Englewood Cliffs, New Jersey: Prentice-Hall Inc.

Jagger, J. (1981). Near-UV Radiation Effects on Microorganisms. *Photochemical and Photobiology , 34*, 761-768.

King, G. F., & Kuchel, P. W. (1994). Theoretical and Practical Aspects of NMR Studies of Cells. *Immunomethods , 4*, 85-97.

Levitt, M. H. (2006). *Spin Dynamics, Basics of Nuclear Magnetic Resonance.* Chichester, England: John Wiley & Sons Ltd.

Madigan, M. T., Martinko, J. M., & Parker, J. (2003). *Brock Biology of Microorganisms* (10th Edition ed.). Upper Saddle River, NJ: Pearson Education, Inc.

Marnett, L. J. (1998). Lipid peroxidation - DNA damage by malondialdhyde. *Mutation Research , 424*, 83-95.

Matsumura, Y., & Ananthaswamy, H. N. (2002). Short-term and long-term cellular and molecular events following UV irradiation of skin: implications for molecular medicine. *Expert Reviews in Molecular Medicine* (4), 1-22.

Mikhailenko, V. M., Philchenkov, A. A., & P, Z. M. (2005). Analysis of 1H NMR-detectable mobile lipid domains for assessment of apoptosis induced by inhibitors of DNA synthesis and replication. *Cell Biology International , 29*, 33-39.

Morliere, P., Moysan, A., & Tirache, I. (1995). Action spectrum ffor UV-induced lipid peroxidation in cultured human skin fibroblasts. *Free Radical Biology and Medicine , 19* (3), 365-371.

Philipp Selenko, G. W. (2007). Looking into live cells with in-cell NMR spectroscopy. *Journal of Structural Biology* , 224-253.

Selenko, P., & Wagner, G. (2007). Looking into Live Cells with In-Cell NMR Spectroscopy. *Journal of Structural Biology , 158*, 244-253.

Serber, Z., Keatinge-Clay, A. T., Ledwidge, R., Kelly, A. E., Miller, S. M., & Dotsch, V. (2001). High-Resolution Macromolecular NMR Spectroscopy Inside Living Cells. *Journal of the American Chemical Society , 123*, 2446-2447.

Sinha, R. P., & Hader, D. P. (2002). UV-Induced DNA Damage and Repair: A Review. *Photochemical & Photobiological Sciences , 1*, 225-236.

Thanbichler, M., Wang, S. C., & Shapiro, L. (2005). The Bacterial Nucleoid: A Highly Organized and Dynamic Structure. *Journal of Cellular Biochemistry , 96*, 506-521.

University of Wisconsin, Department of Biology. (2010). Retrieved from Biological Magnetic Resonance Data Bank: http://www.bmrb.wisc.edu/

Veale, M. F., Roberts, N. J., King, G. F., & King, N. J. (1997). The generation of 1H-NMR-detectable mobile lipid in stimulated lymphocytes: relationship to cellular activation, the cell cycle, and phosphatidylcholine-specific phospolipase c. *Biochemical and Biophysical Research Communications , 239*, 868-874.

Vermeulen, N. (2006). *The effects of ultra violet and visible light on bacterial survival.* Thunder Bay: Lakehead University.

Vermeulen, N., Keeler, W. J., Nandakumar, K., & Leung, K. T. (2007). The Bactericidal Effects of Ultraviolet and Visible Light On Escherichia coli. *Biotechnology and Bioengineering , 99*, 550-556.

Zhang, X., Rosenstein, B. S., Wang, Y., Lebwohl, M., & Wei, H. (1997). Identification of possible reactive oxygen species involved in ultraviolet radiation-induced oxidative dna damage. *Free Radical Biology & Medicine , 23* (7), 980-985.